

RUPRECHT KARL UNIVERSITY OF HEIDELBERG

BACHELOR THESIS

**Comparing fluorescence and bioluminescence
microscopy regarding the effect of
autofluorescence in *C. elegans***

Author:

Lorena Puhl

Supervisors:

Prof. Dr. Michael Krieg
Prof. Dr. Michael Hausmann
Prof. Dr. Jürgen Hesser

*A thesis conducted in fulfillment of the requirements
for the degree of B.Sc. Physics*

at the

Institute of Photonic Sciences
Neurophotonics and Mechanical Systems Biology Research Group

March 10, 2021

Abstract

This research project aims to compare the features of bioluminescence and fluorescence microscopy regarding the disturbing effect of autofluorescence over time. Two transgenic strains of *Caenorhabditis elegans* with mNeonGreen-labelled touch receptor neurons are imaged at different ages. The impacts of the imaging technique, genetics, body-parts and imaged wavelength ranges are discussed. On one hand, images obtained using fluorescence and bioluminescence microscopy, as well as their spatial intensity distributions are compared for gradually ageing animals. Most prominently, they portray a neuronal signal, which is gradually covered by a veil of autofluorescence in the particular case of fluorescence microscopy. On the other hand, bioluminescence methods feature a consistently visible neuron, regardless of the sample's age.

In the further course of the evaluation, the behaviour of autofluorescence over time is quantitatively assessed by evaluating the samples' total intensities. This procedure was separately conducted for extrachromosomal and integrated strains, as well as for tails, bodies, mNeonGreen-spectra and mCherry-spectra. It allows to draw conclusions on how the denoted features influence autofluorescence over time. The most general pattern is portrayed by an increasing autofluorescence for ageing samples. Diving into more detail, mCherry-wavelengths and tails of *C. elegans* both feature lower intensities than their respective counterparts. Furthermore, differences between the two different strains are noted in terms of data-variability, is higher for extrachromosomal strains.

Finally, autofluorescence and signal strength are simultaneously assessed by evaluating the neuron-to-autofluorescence-ratio over time. The general trend is illustrated by a decrease over time. In terms of data-variability, the already mentioned conclusions are also drawn in this case. However, this time the ratios for the tails and bodies of *C. elegans* do not feature any difference.

The most important conclusion is a better suitability of bioluminescence microscopy for ageing samples. Furthermore, fluorescence images may feature better results, when conducted in the mCherry wavelength range, as well as when analysing tissues in the tails of *C. elegans*.

Declaration of authenticity

I herewith declare, that this thesis is my own, and that no other sources than those cited have been used.

Lorena Puhl



Barcelona,
March 10, 2021

Acknowledgements

I would herewith like to thank the following persons for their valuable support, help and advice:

The NMSB lab:

Prof. Dr. Michael Krieg
Dr. Adriana González
Dr. Montserrat Porta
Dr. Ravi Das
Dr. Frederic Català Castro
Dr. Shadi Karimi
Dr. Aleksandra Pidde
Neus Sanfeliu
Lynn Lin
Nawaphat Malaiwong

The University of Heidelberg:

Prof. Dr Michael Hausmann
Prof. Dr. Jürgen Hesser

Contents

1	Introduction and Motivation	5
2	Background	6
2.1	Caenorhabditis elegans	6
2.2	Fluorescence	7
2.2.1	Jablonski diagrams of fluorophores	7
2.2.2	Fluorophores and fluorescent proteins	9
2.2.3	Properties of fluorophores	11
2.3	Fluorescence microscopy	12
2.3.1	Fluorescence microscopes	13
2.3.2	Resolution in fluorescence microscopy	13
2.3.3	Fluorescent tags	14
2.3.4	Disadvantages of fluorescence microscopy	16
2.4	Bioluminescence	17
2.4.1	Physical properties of bioluminescence	17
2.4.2	Bioluminescence imaging	17
2.4.3	Nanolanterns	18
2.4.4	Bioluminescence Resonance Energy Transfer (BRET)	19
3	Methodology	22
3.1	Research question	22
3.2	Experimental approach	22
3.2.1	Sampling	22
3.2.2	Imaging and measurements	22
3.3	Analysis	23
3.3.1	Preprocessing	23
3.3.2	Quantitative analysis	25
4	Evaluation	29
4.1	Qualitative comparison of fluorescence and bioluminescence microscopy	29
4.2	Quantitative evaluation of autofluorescence	34
5	Discussion	37
6	Summary and Outlook	40
7	Appendix	41

1 Introduction and Motivation

What is science? It is the art of shedding light on the principles of nature, and understanding our surroundings and the world we live in. Since the earliest age of humanity, such questions were omnipresent. Answers were sought for in stories and religion, but also in how Nature presented itself. Observation was the first step towards science, followed by the attempt to explain and understand what had been witnessed. Consequently, watching and seeing are key-stones for grasping Nature. This idea lead to the development of microscopes, which initially were represented by a composition of tubes and lenses. In 1590, Zacharias Janssen and his son Hans set in motion the attempt to enlarge matters of nature, using such a construct. One hundred years later, in 1676, the first living cells were observed by Antonie van Leeuwenhoek. He was the first to shed light onto the outlines of bacteria, using a 270-fold magnification. The technique of microscopy rapidly improved throughout history until today, and continues evolve[1].

In the 20th century fluorescence microscopy became a new powerful tool for studying biological matter[2]. However, around 2010 the use of bioluminescence for depicting features hidden to the bare eyes emerged[3]. It is a fairly new idea, that might in future replace the current standard, i.e. fluorescence microscopy, since the latter technique features several drawbacks, such as so-called autofluorescence, to which bioluminescence microscopy is not subjected. This research project aims to shed light onto the contrasting features of both imaging methods, by giving special attention to autofluorescence. For this purpose, *C. elegans* is used as an experimental model[4].



Figure 1: Antonie van Leeuwenhoek[1]

2 Background

2.1 *Caenorhabditis elegans*

Caenorhabditis elegans is a small nematode, that gained particular attention in 1963, when Sydney Brenner used it as a model for his research in developmental biology[4].

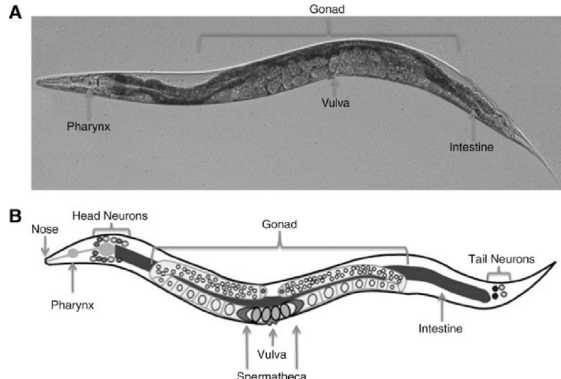


Figure 2: Anatomy of *C. elegans* [5]

Brenner was the first to study the animal's DNA[6], until it finally became the first multi-cellular organism with a fully sequenced genome in 1998. This knowledge made it particularly suitable for research making use of genetic manipulation. Its uniqueness is further underlined by being the only organism with fully known neuronal structures[7]. In short, *C. elegans* is a notably powerful model for conducting research in the field of genetics and developmental biology, which has contributed to the award of six Nobel Prizes.

Furthermore, some properties of *C. elegans* also make it particularly suitable for this project. On one hand, its fully known genome allows for straightforward genetic manipulation. Also, its transparent cuticle makes it particularly easy to image inner tissues and organs, while its short life-span of approximately two weeks (at 25 °C) makes the observation of its ageing process particularly comfortable[8].

The worm's development is categorised in stages before and after adulthood and egg-laying. Before they reach fertility, the nematodes undergo phases labelled from *L1* to *L4*, as depicted in the image below. Subsequently, they reach adulthood, and begin to lay eggs. Worms continue to reproduce for up to two weeks at low temperatures of 16 °C, before they reach the stages of old adulthood, and finally die[8].

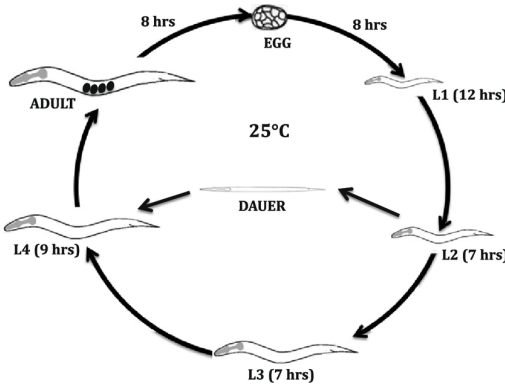


Figure 3: Development stages of *C. elegans* at 25 °C until adulthood[9]

For the sake of this project, it is necessary to shed some light on a few of the animal's anatomical features. Those, which will be discernible over the course of this investigation are depicted below:

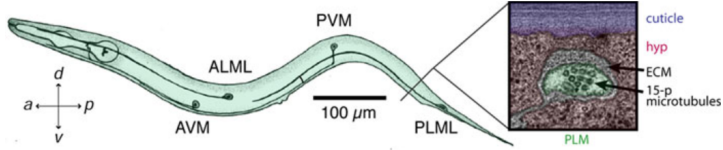


Figure 4: (left) Cell bodies and neuronal processes of the touch receptor neurons. (right) Electron micrograph of a PLM neuron[10].

C. elegans features three touch receptor neurons in its posterior part, and three others in the anterior body. Depending on their exact location, they are further differentiated into one ventral and two lateral neurons in each body-part (ALML, ALMR, AVM, PLML, PLMR and PVM). They are tightly connected to the nematode's cuticle, wrapped by hypodermal cells, and encircled by an electron-dense extracellular matrix[11]. The neuron's direct contact with the worm's cuticle determines its purpose as mediator of touch signals. More precisely, it fires upon sensation of external forces on the worm's surface or internal ones during locomotion, and herewith initiates the animal's response mechanism[10].

2.2 Fluorescence

The term "fluorescence" was used for the first time in history by Sir George Gabriel Stokes in his paper "On the Change of Refrangibility of Light"[12] in 1852. He examined the ability of fluorite to absorb light in the UV-range, and hereafter to emit it in the visible spectrum. As this phenomenon revealed itself to him by the element of fluorine, Stokes coined the new term "fluorescence", which is used until today.

In general, every process describing an atom or molecule, that emits light is denoted as "luminescence". It verbalises an electron's transition from an excited state A^* to the ground state A . According to how the electron's excitation occurred, one discerns different types of luminescence. Chemical luminescence, for instance, describes the emission of light of an electron, that drew excess energy from a chemical reaction. On the other hand, if a photon is responsible for the electron's excitation, one speaks of fluorescence or phosphorescence[2].

Prior to the discovery of quantum mechanics, the latter two phenomena were distinguished by the observation, that fluorescent matter seemed to almost instantaneously loose its characteristic feature, as soon as the excitation light-source was omitted. To the contrary, phosphorescent light emission perpetuated for a certain amount of time. Causing this contrast are the different life-times of both processes. Whereas fluorescence lies between $1ns$ and $10ns$, phosphorescence is characterised by a significantly longer life-time in the range of ms to s [13]. Nevertheless, one has to point out, that long-lasting fluorescence and short-lived phosphorescence do also exist.

2.2.1 Jablonski diagrams of fluorophores

Jablonski diagrams were first introduced by the polish physicist Aleksander Jabłoński in 1933, to illustrate the absorption and emission process of light in luminescent matter.

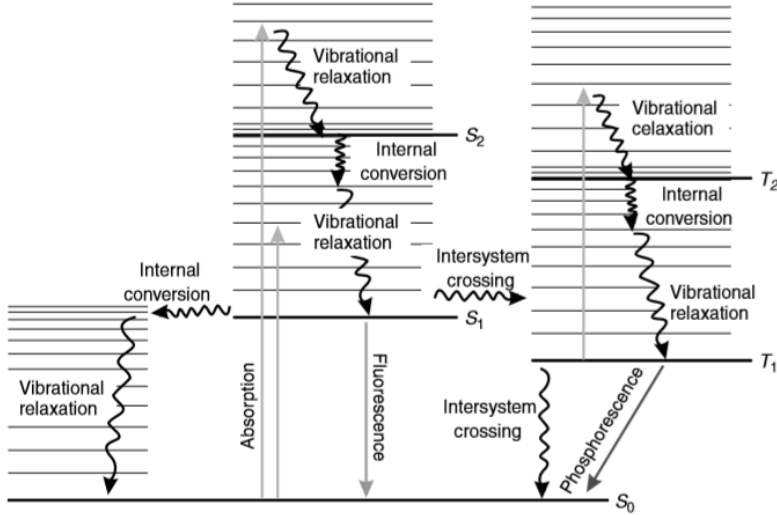


Figure 5: Jablonski diagram[14]

Generally speaking, the ground state of fluorophores is composed of a singlet state. The total spin of both electrons adds up to $S = (+\frac{1}{2}) + (-\frac{1}{2}) = 0$, giving rise to a multiplicity of $2S + 1 = 1$. Resultingly, both electrons feature opposite spins $\uparrow\downarrow$ and $\downarrow\uparrow$. As they are indistinguishable particles, their wave-function is subject to exchange symmetry, indicating, that $|\psi(1, 2)|^2$ has to be constant for every manner of designation. Furthermore, the Pauli-principle requires an anti-symmetric wave-function for a system of fermions with spin $s = 1/2$. Both conditions translate to the $\psi(1, 2) = \frac{1}{\sqrt{2}}(\uparrow\downarrow - \downarrow\uparrow)$ for the wave-function of two electrons in the ground state[15].

The process of excitation with a mean duration of $10^{-15}s$ is the fastest depicted in the Jablonski-diagram. By absorbing a photon, electrons are transferred from the HOMO (Highest Occupied Molecular Orbital) to the LUMO (Lowest Unoccupied Molecular Orbital). These are denoted by the singlet state S_0 and the energetically next-highest singlet state S_1 . As a consequence of conservation of angular momentum, exciting electrons into the triplet state T_1 is impossible[16].

The relaxation of electrons is governed by numerous different processes. On one hand, vibrational relaxation denotes the loss of energy by transferring it to the molecule's or atom's inner vibrational modes. This behaviour is owed to the change of electronic configuration after the absorption of a photon. Consequently, the nuclei must relocate themselves according to the molecule's new energetic conditions, inducing molecular vibrations[14].

Alternatively, electrons may also be subjected to internal energy conversions to a lower singlet state first, before finally loosing further energy until the lowest vibrational level of the electronic state is reached. Such processes are designated as non-radiative and illustrated using undulating arrows in the Jablonski-diagram.

On the other hand, relaxation can also arise through radiation of energy in form of electromagnetic waves. When talking of luminescence, this is the process alluded to. More precisely, electrons can undergo different transitions during the process of luminescence.

On one hand, fluorescence determines the transition of $S_1 \rightarrow S_0$, which most commonly lasts between $10^{-10}s$ and $10^{-7}s$. According to the Kasha-rule, radiation exclusively occurs from the lowest excited state singlet S_1 . For higher excited states S_1* energy-loss is dominated by non-radiative processes. This phenomenon gives rise to the so-called stokes-shift, which refers to the wavelength-difference between the absorption and emission spectra of luminescent matter. As during the electron's relaxation, only a part of the energy is transferred by radiation, the emitted light is always energetically lower, than the absorbed light[17].

On the other hand, electrons may also shift to an excited triplet state T_1 . During this process, a spin-

flip occurs, resulting in a total spin of $S = 1$. One obtains $2S + 1 = 3$ possible anti-symmetric electronic states composed of $\psi(1, 2) = \uparrow\uparrow$, $\psi(1, 2) = \downarrow\downarrow$ and lastly $\psi(1, 2) = 1/\sqrt{2}(\uparrow\downarrow - \downarrow\uparrow)$. This process takes place without any light-emission, and is therefore forbidden according to the conservation of angular momentum. However, the electromagnetic interaction between the electron's spin and the magnetic field, generated by the movement of charged particles (spin-orbit coupling), allows for a tiny probability, that this process may still occur. Once electrons undergo the mentioned spin-flip, the ground state of T_1^* is reached through further vibrational energy loss.

Once the ground state T_1 is reached, electrons finally shift to the ground state S_0 , while simultaneously emitting light, called phosphorescence. Eventually, the low likeliness of a spin-flip unravels the reason for the significantly higher life-time of phosphorescence, lying between $10^{-6}s$ and $10s$. One may slightly increase the probability, by adding heavy atoms to the luminescent molecule, and herewith strengthening the spin-orbit coupling[18].

2.2.2 Fluorophores and fluorescent proteins

Although fluorescence seemed to be a known phenomenon in nature and the animal kingdom, true understanding of the exact components, that demonstrated this feature only started in the year of 1955. The two biologists Davenport and Nicol managed to discern the luminescent tissue of *Hydromedusea*, a subclass jellyfish[19]. The feature responsible for the tissue's fluorescence was finally identified in 1962 by Osamu Shimomura[20] as a protein, later called *Green Fluorescent Protein* (GFP). GFP was the first fluorescent protein to be discovered and investigated, making it the key-stone for the development of other fluorescent proteins and techniques used in fluorescence microscopy.

As GFP is the first fluorescent protein to be discovered and the most widely spread, it will be used as a model to explain the functioning of fluorochromes.

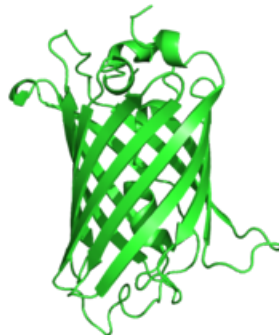


Figure 6: Structure of GFP[21]. Its tertiary structure is a barrel, containing the chromophore in its centre. The latter compound is made of a short chain of altered amino-acids, namely Ser - dehydro Tyr - Gly[22].

Before diving into further detail, it is necessary to clarify the structure of a fluorochrome. It consists of the *fluorophore*, GFP in this case, which in turn is the fusion of a protein and the light-emitting component, the *chromophore*. It is possible to fuse GFP to further protein-structures, creating a *Hybrid-protein*[23].

Understanding the physics of fluorescent proteins requires a deeper look on the chromophore. It is the site of the energy transitions outlined before, and therefore the centre-point of light-emission. Characteristic for such a chromophore is the conjugated π -electron resonance system. It describes the overlap of p -orbitals, allowing π -electrons to freely move across the resulting composition. Such features are found in double and triple bonds. Additionally, the designated bonds are able to alternate between double and triple structures, resulting in a conjugated system. Such a molecular structure is exemplified below.

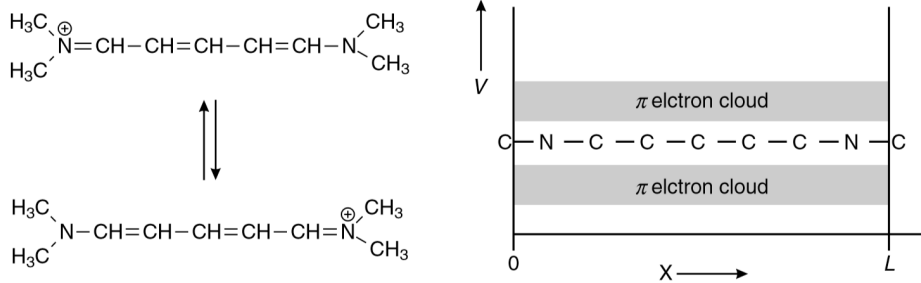


Figure 7: (left) resonance structures of a cyanine dye (right) π -electron resonance system in a simplified potential V of length L [14]

In general, π -electrons of such systems are weaker bound than their σ -counterparts. This is rooted in their parallel structure to the molecule's binding axis, leading to less overlap between the individual π -orbitals. Consequently, the excitations $n \rightarrow \pi^*$ and $\pi \rightarrow \pi^*$ necessitate less energy. To approximate the wavelength needed for such a transition, the absence of interaction between the π -electrons is assumed. This translates into the quantum mechanical *particle in a box model*, whose Schrödinger-equation is easily solved by

$$\psi_n = \sqrt{\frac{2}{L}} \sin\left(\frac{n\pi x}{L}\right). \quad (1)$$

Here, n designates the quantum number, L the length of the molecular box, m the electron's, h the Planck's constant and x the spatial variable.

The Eigenvalues of the resulting wave-functions define each state's energy as

$$E_n = \frac{n^2 h^2}{8mL^2} \quad (2)$$

Consequently, exciting a π -electron into its next energy-level requires a photon of the energy

$$E_{ph} = E_{\text{LUMO}} - E_{\text{HOMO}} = E_n = \frac{h^2}{8mL^2} (n_{\text{HOMO}}^2 - n_{\text{LUMO}}^2) \quad (3)$$

Considering the ground state of a molecule with N π -electrons, its $N/2$ lowest levels will be filled. Therefore, n_{HOMO} can be replaced by $n_{\text{HOMO}} = \frac{N}{2}$ and n_{LUMO} by $n_{\text{LUMO}} = \frac{N}{2} + 1$.

Finally, one obtains

$$\Delta E = \frac{h^2}{8mL^2} (N + 1) \quad (4)$$

or

$$\lambda_{ph} = \frac{8mc}{h} \frac{L^2}{N + 1}. \quad (5)$$

Hence, the absorption energy of a molecule is solely dependent on the bond-length L and the amount of π -electrons N [14].

Of course, this relationship only gives a first impression of the absorption properties of chromophores. It limits itself to a simplified description of a linear molecule as shown above. However, instead of displaying sharp peaks, the absorption spectra of organic dyes cover a wider wavelength-range. After excitation of a π -electron, the overall distribution of charges in the dye changes, causing changing bond-lengths L . Consequently, the initially sharp excitation energies experience a blur, giving rise to the characteristic spectra of organic dyes. Alluding to GFP, its chromophore and excitation spectrum therefore shows more complex features, as depicted below [24].

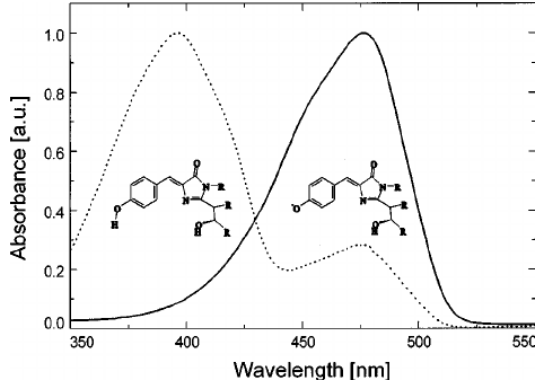


Figure 8: Structure of the GFP chromophore and its excitation and emission spectra[24]

2.2.3 Properties of fluorophores

Finally, fluorophores can be characterised by different features, which make some more suitable than others for each purpose.

Photobleaching

First of all, *photobleaching* refers to the loss of fluorescent properties. It is rooted in non-radiative relaxation processes, or irreversible reactions changing the molecule's absorption and emission properties. On one hand, transition from S_1 to S_0 may occur solely due to internal conversions and vibrational relaxation. Moreover, the fluorochrome's structure also has major impacts on photobleaching. Overall, as higher energetic states are more reactive than their lower counterparts, they are predominantly responsible for photobleaching. An excited electron in the S_1 or T_1 states may absorb a second photon, leading to the fluorophore's ionisation. This transition may be more or less likely, according to the molecule's characteristic transition probabilities, and whether the excitation light matches the shift's resonance frequency. Lastly, the overlap of the $S_0 \rightarrow S_1$ and the $T_1 \rightarrow T_n$ absorption spectra further favour the chromophore's ionisation[14].

Quantum yield

Amongst the most important criteria for choosing a suitable fluorescent dye, are their *quantum yield* Φ_f and *lifetime* τ_f . The first of both properties describes the ratio between the photons absorbed, and subsequently those emitted by fluorescent radiation. It is derived according to

$$\Phi_f = \frac{k_r}{k_r + k_{nr}}, \quad (6)$$

where k_r denotes the radiative rate constant, and k_{nr} its non-radiative counterpart. The latter variable is related to processes, such as internal energy conversions, intersystem crossing and other quantum mechanical processes, that compete with fluorescent radiation[14].

Transition strength

Amongst the most important physical quantities determining the quantum yield, is the *transition strength* between two energy states. It describes the probability for an electron to shift from one orbital to another, by emission or absorption of light. Features, such as the wave-functions of the initial and final states, as well as the nature of the interaction between both functions have a strong impact on how easily electrons can be transferred from one state to another.

To understand the denoted transition in further detail, it can be illustrated by imagining the electrons as a set of electrically charged dipoles. Upon excitation by an electromagnetic wave, energy is transferred, setting them into motion. Their movement can be approximated by that of an harmonic oscillator with a characteristic frequency ν_i . If the excitation frequency lies near the electron's resonance frequency, energy

is transferred, and absorption occurs. The intensity of the designated interaction is described by the *oscillator strength* f_i , which portrays the amount of electrons on a molecule, oscillating with the frequency ν_i . This quantity is used to experimentally investigate the transition strength between two states, and can be determined according to

$$f = \frac{2303}{\pi N_A e^2 n} \int \epsilon(\nu) d\nu \quad (7)$$

The constants m , e , c , N_A , and n denote the electron's mass and electrical charge, the speed of light, Avogadro's constant and the medium's refractive index. Finally, f is determined by considering the entire range of absorption frequencies ν , therefore integrating over the fluorophore's entire absorption spectrum $\epsilon(\nu)$.

In quantum mechanics, the transition strength takes heed of the wave-functions of the initial and final states ψ_i and ψ_f , as well the molecule's dipole strength μ . It can be pictured imaging how significant the spatial overlap between both states becomes, after being exposed to electromagnetic radiation. The transition dipole moment μ_{if} subsequently behaves according to

$$\langle \mu_{if} \rangle = \int \psi_i^* \mu \psi_f dv \quad (8)$$

where $\hat{\mu}$ represents the molecule's dipole as a summation of every electron's dipole it contains, namely $\hat{\mu} = \sum_i q_i \hat{\mu}_i$. The expectation value $\langle \mu_{if} \rangle$ can be determined by integrating over a volume with the volume element dv .

Finally, the resulting transition probability is pictured by the *dipole strength* D_{if} , using

$$D_{if} = |\mu_{if}|^2 \quad (9)$$

[14].

Lifetime

Closely related to the previously discussed physical quantities, the lifetime τ_f portrays the time a fluorescent dye spends in the excited state S_1 , before experiencing energetic relaxation to the ground state:

$$\tau_f = \frac{1}{k_f + k_{nr}} \quad (10)$$

From the above quantities, the decrease of excited fluorophores $[F^*(t)]$ over time can be deduced. Picturing an infinitesimally short pulse of excitation light $\delta(t)$, the following relationship is established:

$$\frac{d[F^*(t)]}{dt} = -(k_f + k_{nr})[F^*(t)] \quad (11)$$

Integrating over $t = 0$ until t gives the subsequent expression for the fluorescence intensity $I(t)$:

$$I(t) = I_0 \exp\left(-\frac{t}{\tau_f}\right) \quad (12)$$

Consequently, the lifetime τ_f can be experimentally determined by measuring the time needed for the initial fluorescence intensity $I(t = 0)$ to drop to the value $1/e I(t = 0)$, after excitation using a δ -pulse[14].

2.3 Fluorescence microscopy

During his efforts to increase the the brightfield-microscope's resolution in 1904, August Köhler suddenly came up with the idea to illuminate his sample using short-wavelength UV light. However, to his biggest disappointment, the acquired image seemed to be more blurry; besides recording the UV light reflected by his sample, he also recorded its fluorescence. With this experiment, August Köhler marked the beginnings of fluorescence microscopy, which, especially in life-sciences, soon became one of the most important imaging techniques[25].

2.3.1 Fluorescence microscopes

Since 1904, fluorescence microscopes have drastically evolved, to meet their numerous purposes. A modern prototype is depicted below.

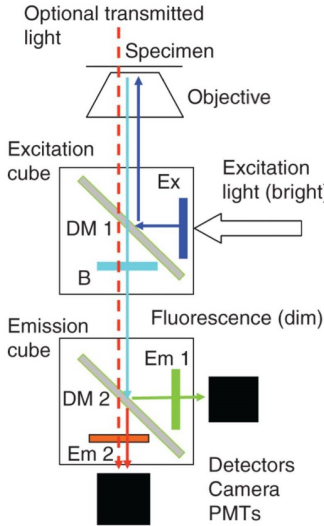


Figure 9: Features of fluorescence microscopes[26]

Essentially, fluorescence microscopes aim to excite a sample, and subsequently record its fluorescence response. According to the fluorescent dye's excitation spectrum, laser-light of a certain wavelength is generated, and directed onto the sample, using a dichroic mirror (DM1). Thereafter, the sample emits fluorescent light, which is redirected onto a detector. However, recording the denoted signal would not yield a satisfying result, as further arrangements have to be made.

On one hand, fluorescent dyes often feature very broad emission and excitation spectra, sometimes causing the spectra of different fluorescent molecules to overlap. In order to primarily excite the fluorescent dye of interest, it is therefore crucial to narrow the laser's wavelength to the peak of the according excitation spectrum. This is achieved by using an excitation filter (Ex), before guiding the light onto the sample.

Furthermore, the light emitted by the sample will not only include its fluorescence, but also scattered light from the laser-beam, as well as additional bleed-through from other fluorophores. As a means to separate the desired signal from additional light, the dichroic mirror (DM1) is specifically tuned to exclusively let through wavelengths from the fluorophore's emission spectrum. Furthermore, a blocking filter is added, enhancing the mirror's purifying effect.

Optionally, samples can be tagged with different fluorescent dyes, when imaging different features at the same time. To detect both signals separately, an additional emission cube, containing a dichroic mirror (DM2) and two emission filters (EM1 and EM2), is added to the light's pathway. The mirror divides both signals, according to their distinct wavelengths, whereas the filters further reduce the recorded signal to the emission peak of the according fluorescent dye[26].

2.3.2 Resolution in fluorescence microscopy

One of the advantages of fluorescence microscopy is that it is not subject to Abbe's diffraction limit. The latter can be understood by visualising the object as a grid of points, which is to be magnified by the microscope. When acquiring the sample's image, it is illuminated by light, which is diffracted after passing through the grid. The Abbe-limit is derived by analysing the emerging diffraction pattern. It is defined by the minimal distance d between two points on the grid, such that the diffraction-maximum of the first is precisely located over the minimum of the other[27]. These considerations lead to the following equation:

$$d = \frac{\lambda}{n \sin(\alpha)} = \frac{\lambda}{NA} \quad (13)$$

n symbolises the refractive index of the immersion medium put into use, λ the wavelength of the light used to illuminate the sample and α half of the objective's opening angle. The product $n \cdot \sin(\alpha)$ is also defined as the numerical aperture NA .

However, the above principle does not apply to fluorescence microscopes. Instead of recording diffracted light from an outer source, the signal is composed of light, emitted by the sample itself. More specifically, fluorescence microscopy yields a diffraction pattern, composed of the emitted light of every single fluorescent molecule found in the sample. To understand the denoted diffraction pattern, one views an ideal light-emitting point, which illustrates a single fluorescent molecule.

According to Huygens's theory, the light emitted from this point, is able to diffract with itself. This phenomenon gives rise to a 3D-diffraction pattern, also called *point-spread-function*. It describes the intensity distribution of light in space, emitted by a single point. On the lateral axis, the denoted pattern is composed of so-called *airy-disks*, as shown in the image below[28]. They are the projection of a 3D-Gaussian on the lateral plane. The distance between the centre point of highest intensity and the neighbouring disc of minimum intensity is determined by $0.61\lambda/NA$. Along the optical axis, the pattern is more widely spread, giving rise to a oval shaped pattern. Consequently, resolution along the optical axis is lower, and the distance between the central maximum and the next minimum is determined by $2n\lambda/NA^2$. Finally, the recorded image is composed of a superposition of every fluorophore's point-spread-function. In order to discern two light-emitters on the focal plane, the same considerations as for the Abbe-limit are applied; the minimum distance d has to be such, that the minimum of the first airy-disc is positioned over the the first minimum of the other. This consideration gives rise to the Rayleigh-criterion below:

$$d = 0.61 \frac{\lambda}{NA} \quad (14)$$

Here, λ designates the wavelength of fluorescence light[29].

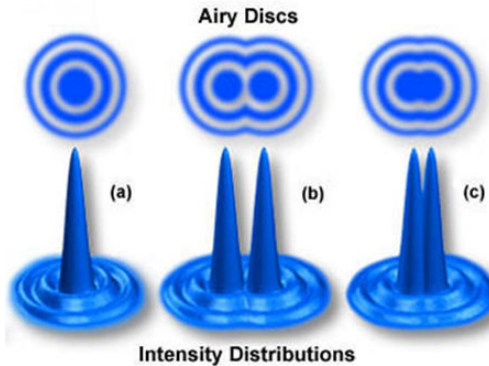


Figure 10: (above) airy discs of two ideal light-emitting points. (down) Gaussian intensity distribution of two ideal light-emitting points [30]

Finally, further phenomena such as spherical and chromatic aberration also take effect on the point-spread function, additionally impairing the minimum resolution.

2.3.3 Fluorescent tags

The second, perhaps more important, advantage of fluorescence microscopy is the possibility to apply specific colour tags to the biologic structures of interest. This allows to discern them from cells and tissues.

The above technique of *fluorescent labelling* can be achieved through numerous approaches[31]. Chemical labelling, for instance, marks the structures of interest by inducing a chemical reaction, which binds the

fluorescent tag to its target. On the other hand, *protein labelling* makes use of short fluorescent tags, which do not disrupt the targeted protein's characteristics, such as protein folding. Using transition metals, these tags are attached to the investigated protein.

Lastly, diving into the specifics of this project, modifying an organism's genome to induce the production of fluorescent proteins in very specific tissues also enables their fluorescent labelling.

Fluorescent labelling in *C. elegans*

MSB557 and MSB651 are two transgenic strains of *C. elegans*, which additionally contain the genetic sequences for *mNeonGreen* and *mCherry*, two fluorescent proteins in the green and red emission ranges respectively. In most of the cases, the denoted DNA is derived from bioluminescent organisms. In such manner, *mNeonGreen* is obtained from the *Branchiostoma lanceolatum*[32], a lancelet living in high underwater depths, and *mCherry* from the *Discosoma*[33] sea anemone.



Figure 11: Structure of mNeonGreen[34]. Its tertiary structure is identical to that of GFP. However, they differ in their DNA-sequence and number of amino-acids (237 and 238 for mNeonGreen and GFP respectively). The chromophore is formed by the tripeptide GYG[35].

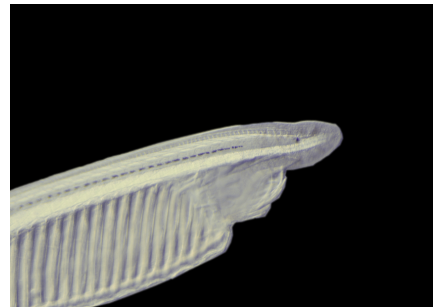


Figure 12: *Branchiostoma lanceolatum*[36]

Fusing a fluorescent protein's DNA to certain promoters from the worm's genome, exclusively stimulates its transcription in specific tissues of *C. elegans*. In the case of the denoted strains, mNeonGreen's sequence is fused to the so-called *mec-4 promoter*, which activates the transcription of the *mec-4*-gene in the worm's touch receptor neurons[37]. This gene encodes the structure for specific channel-proteins, which are crucial for their correct functioning. Consequently, fusing the genetic sequence of mNeonGreen to the above promoter equally enables the fluorescent protein to only be produced in the denoted neurons. In the same manner, the sequence for *mCherry* is attached to the *myo-2 promoter*, responsible for activating the *myo-2*-gene, which encodes myosin-proteins in the worm's pharynx[38].

In more scientific terms, the above mutations are specified using the allele name *mirEx218 [mec-4p::mNG:cNL::let858 3'UTR+myo-2p::mCherry]* for MSB557 and *mirIs58 [mec-4p::mNG:cNL::let858 3'UTR+myo-2p::mCherry]* for the MSB651 strain. Shedding light upon this cryptic notation, the genotypes of transgenic strains are noted by listing all differences with the wild-type's genome. In the present examples, the altered genes are specified by *mirEx218*, where *Ex* denotes an extrachromosomal array, and *mirIs58*, using *Is* to illustrate an inserted array. The implications of the denoted difference will be highlighted in the subsequent paragraph. In the above case, both worms feature the same allele *[mec-4p::mNG:cNL::let858 3'UTR+myo-2p::mCherry]*. Most important for this research project are the notified fusions of the *mec-4 promoter* (*mec-4p*) and a *mNeonGreen-Nanolanterns* (*mNG:cNL*), which will later be described in further detail, as well the joined sequences of the *myo-2 promoter* (*myo-2p*) and the *mCherry* fluorescent protein[39].

Genetically manipulating the described alleles allows to precisely locate fluorescent proteins in the tissues of interest, and therefore to selectively image them. This is showcased by illustrating below fluorescence images if the MSB557 strain, individually selecting the mCherry and mNeonGreen signals.

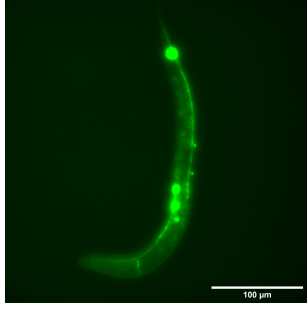


Figure 13: mNeonGreen-labelled touch-receptor neurons in *C. elegans*

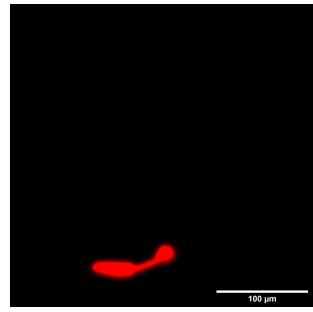


Figure 14: mCherry-labelled pharynx in *C. elegans*

Diving deeper into the genetics of the denoted strains, DNA manipulation can be achieved using different methods. On one hand, extrachromosomal strains, as exemplified by MSB557, are obtained, by injecting plasmids with the desired DNA inside the worm’s germline[40], where they form long concatemers. These are DNA molecules with hundreds[41] of repetitions of the same sequence, also referred to as *transgenic arrays* in this specific case. It is important to note, that the amount of plasmids concatenated to form such an array differs from worm to worm. Furthermore, its expression variability is showcased by enhancement in somatic cells[40], and silencing in germ cells. After injection, the array is mitotically and meiotically transmitted during cell division and reproduction. However, the array’s conveyance is subject to chance, such that not the entire progeny will carry the extrachromosomal array[42]. In a similar manner, transgenic arrays are not always transmitted during mitosis. Consequently, it is not carried by every cell, bringing into existence so-called *mosaic worm*[43]. The above uncertainty also induces increased expression variability among siblings of the same strain, especially for ageing worms, which have gone through more cell divisions[44].

On the other hand, MSB651 denotes a so-called *integrated strain*[45]. It is generated by inserting the above extrachromosomal arrays into the worm’s chromosomes. Typically, it is carried out by inducing double-strand breaks in the DNA, using X-ray or UV light, as well as chemical mutagens[43]. In the case of the denoted strains, *TrimethylIpsoralen (TMP)* was used. Finally, during the DNA’s reparation process, the array is occasionally incorporated into the worm’s genome at a random location. If the denoted process is successfully accomplished, it produces an integrated strain, which leads to a more stable expression of the transgenic gene. Additionally, the gene is fully inherited by the worm’s progeny.

2.3.4 Disadvantages of fluorescence microscopy

Even though fluorescence microscopy comes with numerous advantages, it faces several problems, which need to be addressed.

First of all, *phototoxicity* denotes the damage caused to biological tissues while imaging. As the incidence laser-beam necessitates a power-density in the range of W/cm^2 [46], the transferred energy may initiate photophysical mechanisms, leading to highly reactive products, heat and DNA damage. Furthermore, the fluorescent emission also brings forth damaging free radicals, further harming live tissues.[47]. Along the same lines, fluorescence microscopy is not applicable for imaging live processes, which are directly affected by light, as the incident beam would disturb the investigated phenomena.

Furthermore, *photobleaching*, as discussed earlier, leads to a decrease in fluorescent emission intensities. This gradually impairs fluorescent imaging in its most basic principles.

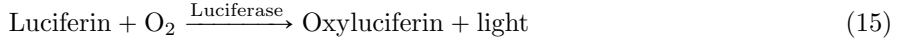
Finally, many biological tissues naturally contain molecules, which emit light upon excitation. This phenomenon is known under the name of *autofluorescence*[48]. When the emission wavelengths coincide with the fluorophore’s emission spectrum, the denoted bleed-through cannot be separated from the sought signal, and

potentially overshadow it. It leads to an increase in background intensities, which subsequently impairs the signal's visibility. The denoted problem is also investigated in this project.

2.4 Bioluminescence

Bioluminescence is the self-reliant production of light by living organisms. Some speculate, that its first written evidence dates back to approximately 1450BC with Moses' "burning bush". Supposedly, the emitted light originated from a bioluminescent fungus infection of the leaves. More well-founded testimonies are provided by Aristotle (384-322 BC), who described the glowing nature of organisms, such as fireflies and glow-worms, as well as that of dead fish or flesh, due to infections with bioluminescent bacteria[49].

The underlying phenomenon of the above description is rooted in chemical reactions, involving proteins and enzymes, which are accompanied by the emission of photons. More specifically, a light-emitting molecule, *Luciferin*, undergoes a catalysed oxidation in the presence of a *Luciferase*. Consequently, bioluminescence is categorised as a type of *chemiluminescence*[50].



2.4.1 Physical properties of bioluminescence

Amongst the most important characteristics of bioluminescence is its quantum yield Φ_B . It is determined by three efficiencies, namely the chemical yield Φ_Y , the excitation efficiency Φ_E and the fluorescence efficiency Φ_F . The first denotes the probability for the Luciferase to undergo the different chemical sub-reactions for forming the final product, Oxyluciferin. The second quantity refers to the fraction of final Oxyluciferin-molecules, which complete the oxidation in an excited energetic state. Solely these molecules are finally able to emit a photon, while transitioning to their ground state. Lastly, Φ_F denotes the previously outlined fluorescence quantum yield. It quantifies the fraction of radiative electron transitions in opposition to the total possible transitions[49].

$$\Phi_B = \frac{n_{\text{emitted photons}}}{n_{\text{oxyluciferin}}} = \Phi_Y \Phi_E \Phi_F \quad (16)$$

2.4.2 Bioluminescence imaging

Bioluminescence may be a promising foundation for developing new imaging techniques, as it does not feature most of the disadvantages fluorescence microscopy is linked to. The self-sufficiency of bioluminescent reactions implies, that a signal can be obtained without excitation light. Consequently, phototoxicity and autofluorescence are nonexistent, and the complex composition of fluorescence microscopes, involving dichroic mirrors and filters, is redundant. Moreover, bioluminescence imaging is a suitable technique for observing processes, which are directly affected by light.

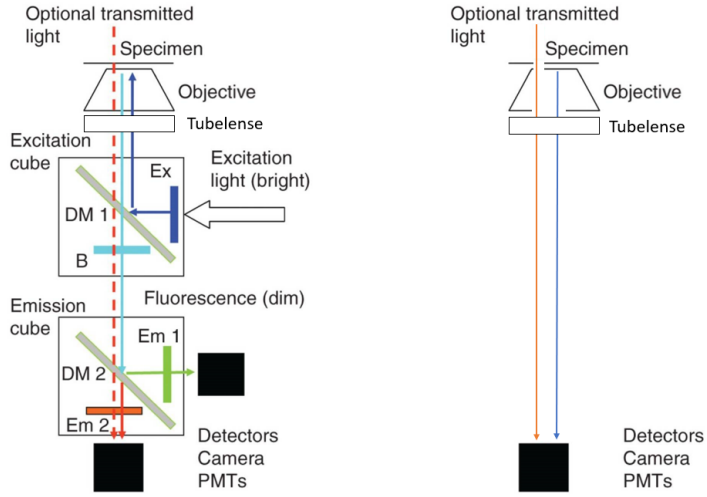


Figure 15: Comparison of a fluorescence (left) and bioluminescence microscope (right). Excitation light, as well as emission and excitation filters become redundant.[26]

However, the above equation characterising the quantum yield in bioluminescence, already portrays its most important shortcoming. Instead of solely being defined by Φ_F , like it is the case for fluorescence imaging, two additional factors come into play. This causes a significant decrease in the total quantum yield of bioluminescence reactions. *Firefly luciferase*, for instance, is characterised by a quantum yield of $\Phi_B = 0.5$ [51], whereas *Renilla luciferase*[52] features an even lower value of $\Phi_B = 0.053$ [53]. Consequently, the power density of bioluminescent emission is $1/10$ [53] of the requirements for fluorescence live cell imaging (approximately $0.1 \mu W/cm^2$).

Altering the structure of the Luciferase to create so-called *nanolanters* is a currently used method to tackle the most challenging shortcoming of bioluminescence.

2.4.3 Nanolanters

In general, nanolanters are fusions of Luciferases with fluorescent proteins. They have already been encountered in the two *C. elegans* strains MSB557 and MSB651 as *mNeonGreen-Nanolanter* (*mNG:cNL*). In this specific case, *mNeonGreen* is fused to the Luciferase subunit (*NanoLuc*) of the deep sea shrimp *Ophophorus gracilirostris*[54]. Through *bioluminescence resonance energy transfer (BRET)*, photons emitted by the Luciferin excite the fluorescent dye, which in turn emits fluorescent radiation in its usual quantum yield and wavelength spectrum. To demonstrate the increased efficiency of nanolanters, the previously mentioned *Renilla Luciferase* coupled with the *Renilla Green Fluorescent Protein* ($\Phi_F = 0.3$), features a six-fold quantum yield[55] and ten-fold power density[46]. Although the mentioned value is still significantly smaller than energy densities achieved with fluorescence ($100 \mu W/cm^2$), the achieved spatial resolution is still comparable with that of fluorescence microscopy. As the latter method features high amounts of noise due to autofluorescence and light bleed-through, its neuron-to-autofluorescence ratio becomes comparable with that of bioluminescence microscopy.

The above increase in brightness is determined by the efficiency of energy transition occurring during BRET. It can be maximised by choosing Luciferases with maximum quantum yield, and coupling them with fluorescent proteins featuring overlapping emission and absorption spectra.

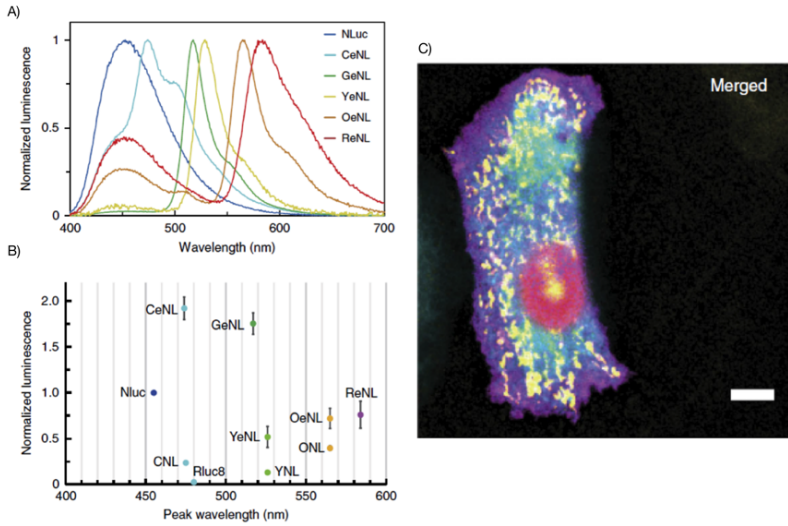


Figure 16: Overview of different nanolanters: Green enhanced nanolanter (GeNL), Cyan enhanced nanolanter (CeNL), Yellow enhanced nanolanter (YeNL), orange enhanced nanolanter (OeNL), Red enhanced nanolanter (ReNL) and NanoLuc (NLuc). (A) Emission spectra of different nanolanters. (B) Bioluminescence intensities of different nanolanters over their wavelength-peak. (C) Multicolor live cell image, featuring NLuc in the mitochondria, CeNL in the endoplasmatic reticulum, GeNL in the nucleoli,OeNL in the plasma membrane and ReNL in the nucleus. [46]

2.4.4 Bioluminescence Resonance Energy Transfer (BRET)

In order to shed further light on how to improve the energy density of nanolanters, it is necessary, to take a deeper look on the mechanisms of Bioluminescence Resonance Energy transfer.

Briefly describing BRET before jumping into further details, it is the interaction of two luminescent molecules, located in a very short distance from each other (within 10nm). This setting establishes strong dipole-dipole bonds, which are the means to transfer energy from the donor to the acceptor without any radiation. In this case, the bioluminescent molecule embodies the donor of energy by means of the oxidation taking place. The acceptor is represented by the fluorescent protein. The designated process very closely linked to Fluorescence Resonance Energy Transition (FRET), which describes the energy transfer between two fluorescent molecules according to the same mechanism.

From a quantum mechanical point of view, direct energy transfer occurs, when the wave-functions of both molecules overlap to a minimum extent. This leads to a direct dipole-dipole interaction between both molecules, which can be described using the following Hamiltonian H :

$$H = H_{\text{mat}}(\text{acc}) + H_{\text{mat}}(\text{don}) + H_{\text{int}}(\text{acc}) + H_{\text{int}}(\text{don}) + H_{\text{rad}} \quad (17)$$

The system portrayed above is characterised by the donor's and acceptor's unperturbed Hamiltonians $H_{\text{mat}}(\text{acc})$ and $H_{\text{mat}}(\text{don})$, the Hamiltonian H_{rad} portraying the radiation, and finally the Hamiltonians $H_{\text{int}}(\text{acc})$ and $H_{\text{int}}(\text{don})$ illustrating the interaction with the denoted radiation field.

Viewing each molecule as a magnetic dipole μ , its interaction with an electromagnetic field becomes

$$H_{\text{int}} = -\mu \mathbf{e}^{\perp}(\mathbf{R}), \quad (18)$$

where \mathbf{e}^{\perp} is the electric field's transverse component to the dipole, which is located at the point \mathbf{R} in space.

Finally, the radiation is illustrated by the according Hamiltonian H_{rad} , as follows:

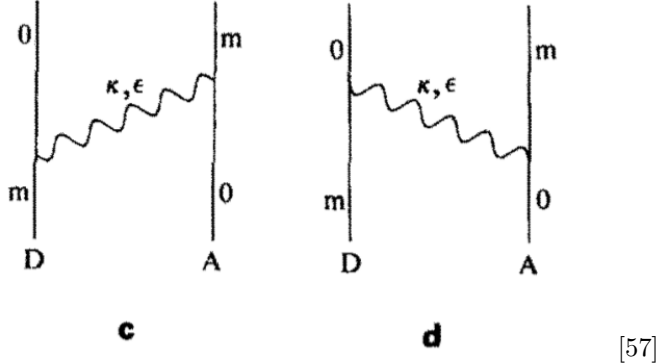
$$H_{\text{rad}} = \frac{1}{2} \int \mathbf{e}^{\perp 2} c^2 \mathbf{b}^2 dr^3 \quad (19)$$

It depicts the square value of an electromagnetic field with the according transverse electric component \mathbf{e}^\perp and magnetic component \mathbf{b} , integrated over the volume $d\mathbf{r}^3$.

Finally, further quantum mechanical observations, including time-dependent perturbation theory, yield the probability amplitude M_{if} for the transfer of energy. It is derived using the second term

$$M_{fi} = \frac{\langle f | H_{\text{int}} | r_a \rangle \langle r_a | H_{\text{int}} | i \rangle}{E_i - E_{r_a}} + \frac{\langle f | H_{\text{int}} | r_b \rangle \langle r_b | H_{\text{int}} | i \rangle}{E_i - E_{r_b}}, \quad (20)$$

where r_a and r_b denote the intermediate states of donor and acceptor respectively. The process is carried out by exchanging a virtual photon, as the mediator of the electromagnetic interaction between both molecules. It is described by the initial i , portraying the donor in an excited state, whereas the acceptor prevails in the ground state. In contrary, the final state f features the donor in the ground state and the acceptor in the excited state[56].



[57]

Figure 17: Dipole-dipole interaction between two molecules by exchanging a virtual photon. m denotes the molecule's excited state, whereas 0 portrays the ground state. A virtual photon with wave vector \mathbf{k} and polarisation vector ϵ is exchanged. (c) represents the donor, while (d) stands for the acceptor

However, once the overlap between both wavefunctions becomes insignificant, direct electromagnetic interaction between both molecules decreases significantly. Instead, energy is conveyed by the emission of an observable photon through radiative energy transfer.

This phenomenon is portrayed by the *Förster critical distance* R_0 , which denotes the distance between donor and acceptor for 50% FRET efficiency. By setting equal the rate of radiative decay by the donor, and that of radiationless energy transfer to the acceptor, one obtains the following formula:

$$R_0^6 = \frac{3f}{4\pi} \int \frac{c^4 \omega^4}{\omega^4 n(\omega)} F(\omega) \sigma(\omega) d\omega \quad (21)$$

Consequently, FRET efficiency is subject to an orientation factor f , the refractive index $n(\omega)$ and the respective donor's and acceptor's energy emission and absorption cross sections $I(\omega)$ and $T(\omega)$.

If both molecules are situated at a lower distance r to each other, FRET is the predominant process for energy transfer. Its efficiency is described by

$$E_{\text{FRET}} = \frac{R_0^6}{R_0^6 + r^6}. \quad (22)$$

The above equation illustrates the rapid decrease to the power of 6, and characterises FRET as a short-distance interaction.

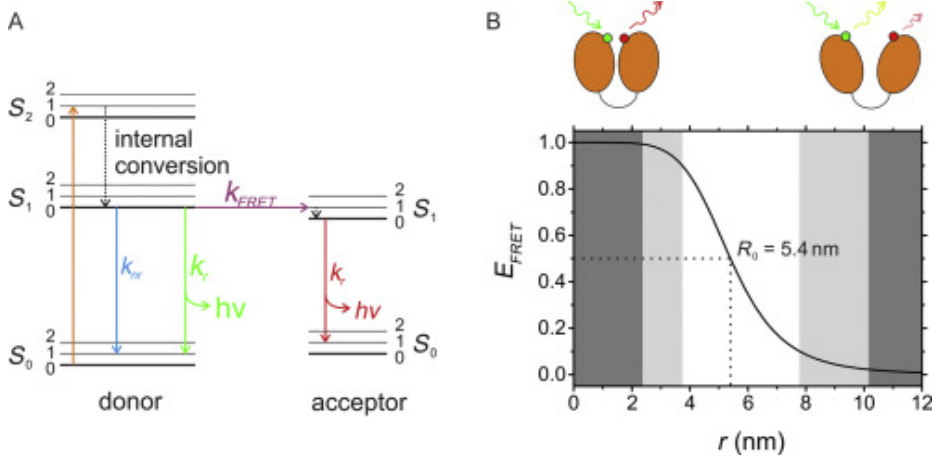


Figure 18: (left) energy conversions during FRET with according rates k . (right) FRET efficiency E_{FRET} over the distance r [58]

As suggested in the image above, the FRET efficiency not only depends on the distance r between both molecules, but also on the rates k of electron energy transitions. Accordingly, E_{FRET} can also be understood as the following relationship between the different transition rates:

$$E_{\text{FRET}} = \frac{k_{\text{FRET}}}{k_{\text{FRET}} + k_r + k_{nr}} \quad (23)$$

k_{FRET} denotes the energy transition rate between both molecules, whereas k_r and k_{nr} correspondingly describe the rates of radiative and non-radiative energy transitions in the donor and acceptor.

Shedding further light on the transition rate k_{FRET} , it is defined by

$$k_{\text{FRET}} = \frac{1}{\tau_D} \left(\frac{R_0}{r} \right)^6, \quad (24)$$

involving the life-time τ_D of the donor's excited state. This last quantity is in turn determined by

$$\tau_D = \frac{1}{k_r + k_{nr}} \quad (25)$$

Combining the three previous equations (21), (20) and (19) finally leads back to equation (18)[57].

3 Methodology

3.1 Research question

This project aims to investigate the features of fluorescence and bioluminescence microscopy, by using *C. elegans* as an experimental model. More precisely, it is focused on the development of a specific feature - autofluorescence - over time, space, wavelength-range and strain, using fluorescence microscopy. These findings are put into contrast with results yielded by methods of bioluminescence.

3.2 Experimental approach

In order to observe the above properties, extrachromosomal MSB557- and integrated MSB651-samples are bred, time-synchronised, mounted and finally imaged. These processes are described in further detail in the following sections.

3.2.1 Sampling

Breeding

In order to breed *C. elegans* in a lab, certain living conditions have to be fulfilled. They are bred at a temperature of 20 °C in petri plates, which are coated by an Agar-layer. It contains several compounds, which are crucial for the worm's healthy development. These include NaCl, Peptone, 5^{mg/ml} cholesterol in ethanol, 1M KPO₄ buffer of pH 6 and 1M MgSO₄[59]. Furthermore, the plates are seeded with the bacteria OP50 for nutrition.

Synchronisation

As this project involves analysis over time, the worms' precise ages at the moment of imaging are evaluated. Consequently, they are expected to hatch and start their development simultaneously, while the time between hatching and imaging is measured. To clearly determine the beginning of the worms' development processes, the strain is bleached and seeded as described below.

The protocol first involves bleaching, of eggs and mothers in the ripe egg-laying stage. As the shells of eggs are more resistant than the mother's cuticle, bleaching them dissolves the old worms, solely leaving behind the eggs. To do so, the petri dishes are washed with an M9 buffer-solution, which is composed of 3g KH₂PO₄, 6g Na₂HPO₄, 5g NaCl, 1ml 1M MgSO₄ to 1L of water. To start the bleaching process, 150 μ l of household bleach (5% solution of sodium hypochlorite) and 100 μ l of 4MNaOH are added to the solution, which contains mothers and eggs. After the worms' cuticles are dissolved, only eggs remain, and the solution is rinsed with an M9 solution. For four times in a row, the solution is centrifuged at 400rpf for 1min. The liquid above the pellet is removed, before adding M9 and shaking the solution[59]. Finally, the rinsed eggs are transferred to a non-seeded petri dish, and left at 20 °C overnight. Without food, the development process of newly hatched worms is not initiated, leaving them in the so-called *arrested L1-state*. Once these are transferred to a seeded plate, their development begins, and the worms' ages can precisely be assessed by noting the time of seeding.

This procedure is applied separately to the two strains MSB557 and MSB651. As MSB557 is an extrachromosomal strain, not every worm expresses the transgenic gene, which is responsible for producing mNeonGreen and mCherry. As a result, wild-type and transgenic worms have to be separated before imaging. They are therefore observed under a fluorescence microscope and manually picked.

Over the course of time, sample worms whose autofluorescence is assessed lay eggs. To separate the samples from their progeny, mothers are therefore transferred every day to new plates.

3.2.2 Imaging and measurements

The imaging process follows two different protocols, depending on which kind of microscopy is conducted. For both, preparing samples involves coating a microscope slide with a 2% Agar layer, on which they are

placed and covered by a cover slip. It is prepared by dissolving $2mg$ of Agar-powder in $10ml$ of mQ water, and heating it to its boiling point. Using a pipette, the obtained liquid is poured onto the microscope slide, and flattened by placing a second one on top.

Fluorescence microscopy

To observe the worms' developments over time, a time-synchronised generation is imaged over a period of approximately two weeks every one to three days. Especially at younger stages, the development process is faster, and therefore requires more frequent imaging. In older stages, it is conducted less often. In total, each strain is imaged approximately five times, using between ten and fifteen samples per acquisition. As fluorescence microscopy requires paralysed worms, a $3mM$ -Levamisol solution is used on the Agar-pad, before placing the samples.

Fluorescence images are acquired using the Leica Microscope DMI8 (L309) with the LasX-interface. As the project involves comparing images over time, it is crucial to maintain the same imaging procedure for every sample. Z-stacks of the worms' entire depths of approximately $0.5\mu m - 1\mu m$ thick slices are taken with an exposure time of $50ms$. For every worm, two hyperstacks are recorded - the first picturing the tail with its three posterior touch-receptor neurons, the second illustrating the worm's gonad and the nearby anterior touch-receptor neurons. Each hyperstack is composed of a brightfield image and two fluorescence images. The latter two are acquired using a GFP filter-cube, that is compatible with mNeonGreen's emission and excitation spectra, combined with a laser of wavelength $485nm$ at 40% intensity. The second imaging process uses a mCherry filter-cube in combination with $575nm$ laser-light of 20% intensity. Each filter cube is composed of an emission and excitation filter, as well as a dichroic mirror. The first setup features a quad band excitation filter, where the $488nm$ window is tuned to mNeonGreen's spectrum. The emission filter is characterised by a $40nm$ window around a wavelength of $510nm$. On the other hand, imaging in the mCherry-range requires a dichroic mirror, that reflects wavelengths below $560nm$, and lets through light with higher wavelengths. The used emission filter is focused on wavelengths around $595nm$ in a $30nm$ range. The mCherry filter cube does not contain any excitation filter, and relies on the laser's wavelength precision. Finally, images are saved in *.tiff*-format.

Bioluminescence microscopy

Bioluminescence images are acquired in a more qualitative manner, by imaging a lower amount of samples per time-point. In general, extrachromosomal strains are suspected to yield a less stable signal. To demonstrate, that bioluminescence is still a valid method for imaging samples of the denoted strain, MSB557 animals are pictured at different ages. However, because not every worm shows a signal during image acquisition, approximately five samples are pictured before obtaining an image with a satisfactory signal-to-noise ratio.

For bioluminescence imaging, the worms are provided with the according light-emitting Luciferin. In this case, a $2.1mM$ Furimazine-solution is used. Additionally, 10% Dimethyl sulfoxide (DMSO) enables the penetration of the worm's cuticle, and a citric buffer-solution decreases the toxicity of the above chemicals. The latter compound is composed of $0.1M$ citric acid, $0.2M$ dibasic sodium phosphate, additional 1% DMSO and 0.05% Triton X-100. Before image acquisition, the worms are placed on the previously mentioned Agar-pad, before pipetting $3\mu l$ of DMSO, $3\mu l$ of buffer and $1 \mu l$ of 7x Furimazine on top. Images are taken with 1s, 5s and 10s exposure times. As this imaging technique solely relies on bioluminescence, no further filters and light sources are needed. Again, images are saved in *.tiff*-format.

3.3 Analysis

In this section, methods for comparing fluorescence and bioluminescence microscopy, as well as for analysing autofluorescence over time, wavelength-range and body-part in *C. elegans* are described.

3.3.1 Preprocessing

First and foremost, images are edited before any further analysis is conducted. *Fiji* or *ImageJ* is an open-source software package developed by the National Institutes of Health (NIH). It is frequently used in

medicine and life-sciences to evaluate heavy images saved in bio-formats, such as *.tiff*-formats.

Using *Fiji*, z-stacks are first projected to a single image, using the maximum-projection algorithm: For every pixel, the stack is swept to find the image, which contains the pixel's highest intensity-value. Doing so for every pixel yields a single image with exclusively maximum intensities.

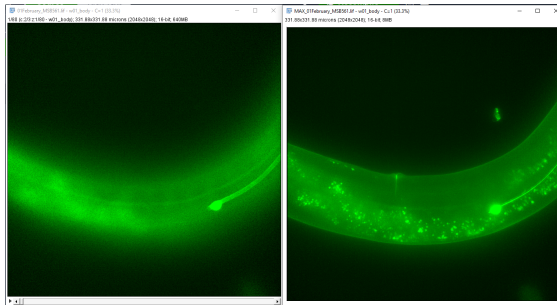


Figure 19: (left) first slice of z-stack. (right) z-maximum-projection of z-stack

Furthermore, the worm's body is straightened using the according segmented line-tool in *Fiji*. In doing so, the axis passing through the worm's neuron is traced, using a line-width of 1500 pixels, before the straightening algorithm is finally applied. Lastly, the GFP-channel is saved using a green colour-map, whereas the mCherry-channel is saved in the red colour-map.

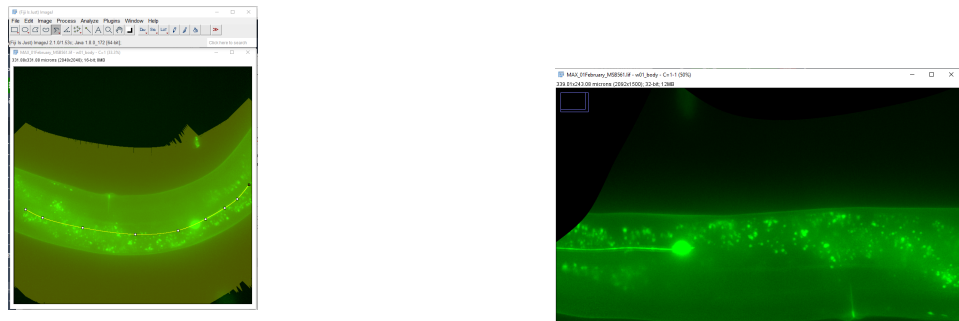


Figure 20: Straightening process in *Fiji*: Using the *segmented line* selection tool with a width of 1500 pixels, a line is drawn across the neuron (if visible). Finally, the worm is straightened along the designated line.

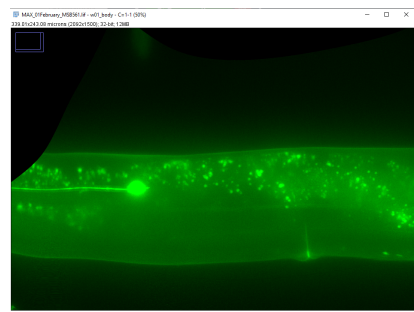


Figure 21: Straightened image.

Furthermore, for determining the *neuron-to-autofluorescence ratio* discernible neurons are individually selected. To do so, the slices in each z-stack containing the neuron are individually selected and rendered into a maximum projection. Applying the same method as above, the neuron is traced and straightened, using a line-width of 25 pixels, before finally saving it to a different file.

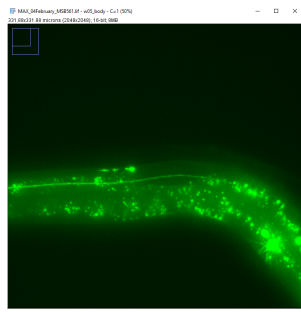


Figure 22: maximum projection of entire z-stack.

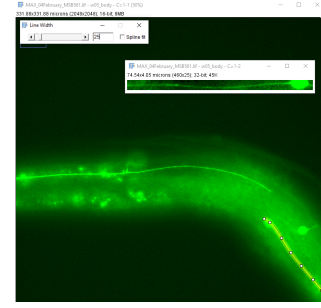


Figure 23: z-projection of planes containing the neuron. The neuron is being selected, straightened and saved to a separate file.

3.3.2 Quantitative analysis

Once preliminary image processing is completed, quantitative analysis using *Python* is finally conducted.

Spatial intensity distribution

The aim of the quantitative analysis is to, first of all, generate a spatial intensity profile over both axes. This approach graphically illustrates the neuron-to-autofluorescence ratio for every worm, and generates a tangible overview of how it develops over time. It is conducted for different strains and excitation-spectra for comparison. Furthermore, illustrating in the same graph the spatial intensity distributions of equal age samples, depicts the biological variability in a population, and may also lead to interesting insights.

The following graph exemplifies the purpose of graphically illustrating such a spatial intensity distribution. A worm's body-area near its gonad is depicted below, which shows autofluorescence, as well as the neuron's signal. The graph next to it exhibits the intensity yielded by averaging the pixels over the image's entire width. This value is plotted over the variable *ypixel*, which describes the image's height from top to bottom. Therefore, *ypixel* = 0 defines the top-most pixel. In this example, a peak at *y* = 800 is pictured, demonstrating the significantly higher intensity of the neuron compared to the worm's remaining body. The more values of peak and body differ from each other, the higher the neuron-to-autofluorescence ratio, quantitatively describing the neuron's visibility in a sea of autofluorescence. This approach is also applied to bioluminescence images, depicting the difference in neuron-to-autofluorescence ratios between both microscopy techniques.

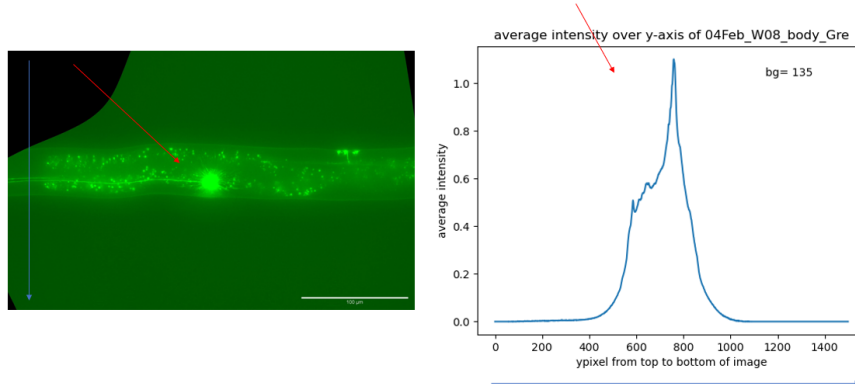


Figure 24: (left) Fluorescence image of a worm's body-area near its gonad with a discernible neuron. The y-axis is illustrated using a blue arrow. (right) Spatial distribution of the mean intensity along the y-axis. A peak specifies the neuron's position, marked by a red arrow.

In order to obtain a spatial intensity distribution as shown above, the straightened worm-image is first read into an array of columns. Subsequently, the mean of every column's pixels with the same indices is evaluated. In this case, the index represents the y-coordinate. This method yields a graph similar to a Gaussian curve, where the baseline is determined by the background, and the bell-like shape represents the worm's fluorescence. This property is used to determine the background-value, using a Gaussian fit, as depicted below.

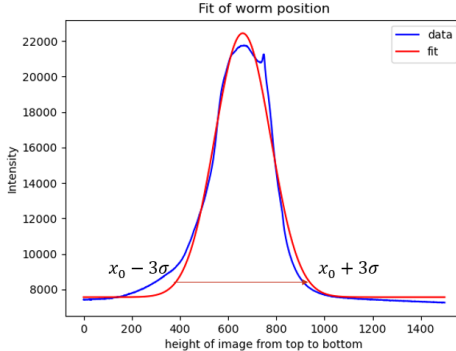


Figure 25: Averaged spatial intensity over the y-axis. A Gaussian is fitted to the data. Its baseline represents the computed background value. The worms y-coordinates are determined by the range $[x_o - 3\sigma, x_o + 3\sigma]$, where x_o designates the Gaussian's median and σ the standard deviation.

However, a small peculiarity has to be taken into account; as the straightening process creates "black spots" with zero-value pixels in the image, including these pixels into the calculation of mean values, falsifies the result. Therefore, only columns, which do not contain any zero-value pixels are used for plotting, fitting and finding the background, as is depicted below.

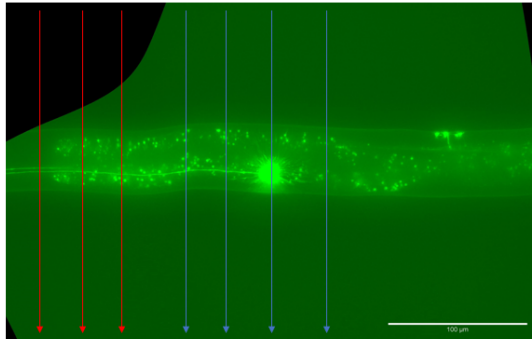


Figure 26: Not every column is utilised to determine the average spatial intensity, used for the Gaussian fit. The red arrows indicate those, which contain zero-value pixels. These are provisionally excluded from the calculations.

Once the sought-for estimate is found, every zero-value pixel is set to this constant. For illustrating the final graph as shown in figure 24, the mean column is determined once more - this time including every column of the picture's entire width. Finally, as backgrounds differ from image to image, a reliable comparison between different data-sets is only achieved by illustrating signal-to-background ratios $signal - background / background$. Figure 24 illustrates the cited fraction composed of the mean column divided by its background.

The same method is brought into play for finding the average intensity over the x -axis. Instead of columns, every line is read into a set of arrays, whereby zero-value pixels are altered to the background variable. This time, the x -coordinate is represented by the lines' indices, and the average line is calculated by determining

the mean of every same-index pixel. Putting this mean in relation to the image's background, and plotting it over every index illustrates the spatial intensity distribution over the x -axis. In this case, $x = 0$ represents the left-most pixel.

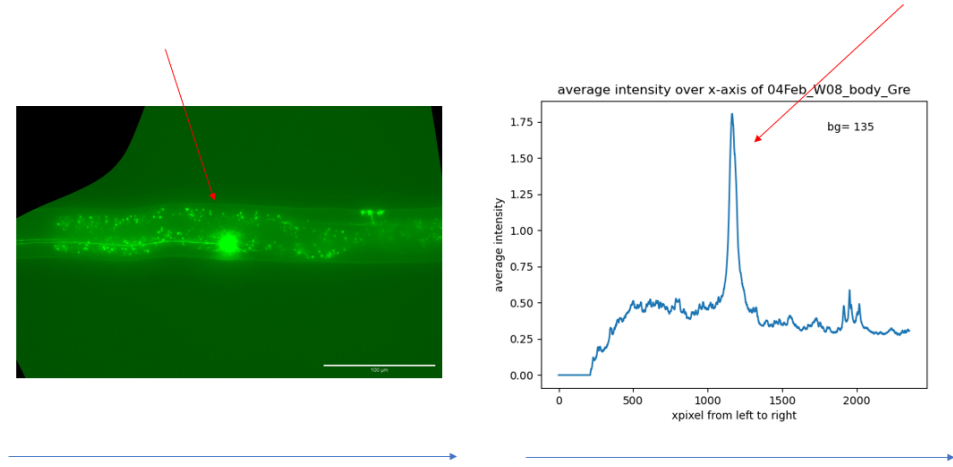


Figure 27: (left) fluorescence microscopy image of a worm's mid-body area. Using a blue arrow, the image's x -axis is denoted, while a red arrows marks the touch-receptor neuron. (right) Respective spatial intensity distribution over the x -axis. The x -axis is denoted using a blue. A significant peak, at the the neuron's x -coordinate is marked by a red arrow.

Total autofluorescence over time

After illustrating autofluorescence over space, it is subsequently described over time. For this purpose, the worm's total intensity is evaluated and illustrated with respect to its age. Again, this approach is also valid for comparing the development of autofluorescence in different strains, excitation-spectra and body-parts. However, as bioluminescence images do not show any autofluorescence, this part of the analysis is solely sensible for fluorescence images.

To shed light upon how the total autofluorescence is determined, the formerly mentioned Gaussian fit, illustrated in figure 25 is called to mind. The indices in the range of $[x_0 - 3\sigma, x_0 + 3\sigma]$ determine the exact y -coordinates of the worm's position in the image. To determine the total autofluorescence, the formerly calculated intensity distribution over the y -axis, as depicted in figure 24 is looked back upon. It is determined by summing all intensity values in the graph, that lie in the specified range, and thereafter dividing it by its width. Finally, the result is plotted over the worm's age at the moment of image acquisition.

To push the analysis even further, the obtained values for worms of the same acquisition set are statistically evaluated. For each moment of imaging, the median values and median deviations of all samples are determined and depicted. Doing so sheds light on how the variability of autofluorescence develops over time.

As an aside, autofluorescence only weakly emerges in the very tip of the worm's tail, where the two neuronal cell-bodies are typically located. However, as this project aims to asses the influence of increasing autofluorescence on the denoted signal, this would lead to a falsified result, untruthfully featuring a neuronal signal, which dominates over the increasing autofluorescence. Therefore, while evaluating the worm's tail, the worm's image is cropped, to exclude the neuronal cell-body. Instead, the signal is solely denominated by its axon.

Neuron-to-autofluorescence ratio over time

Finally, a last method to quantify the signal's visibility is the so-called *neuron-to-autofluorescence ratio*.

It is determined, by evaluating the neuron's intensity, and dividing it by the previously calculated total intensity of the entire worm. Analysing the neuron's image, the picture is again interpreted as a set of columns, which are averaged, to obtain the mean intensity at every y -position. Adding every pixel, and dividing the total value by the image's width approximates the neuron's intensity. It is then subtracted and divided by the background determined earlier.

On a side note, not every worm features a discernible neuron, as the signal is sometimes covered by high autofluorescence intensities. In theory, this is translated into a neuron-to-autofluorescence ratio of zero. To imitate this behaviour during the evaluation, a background area, located outside of the worm, is used to replace the required neuron's image in the course of the calculations.

4 Evaluation

After preliminary reflections, experimental procedures and preparatory processing are carried out, conclusions are finally drawn.

4.1 Qualitative comparison of fluorescence and bioluminescence microscopy

Qualitative observation of ageing worms, using fluorescence microscopy

Before diving into quantitative analysis, it can be instructive to obtain a figurative understanding of the observed features. For this sake, the evaluation is introduced by a graphical representation of the worm's ageing process. The most representative sample is chosen for every development stage, and put into contrast with the remaining maturity levels.

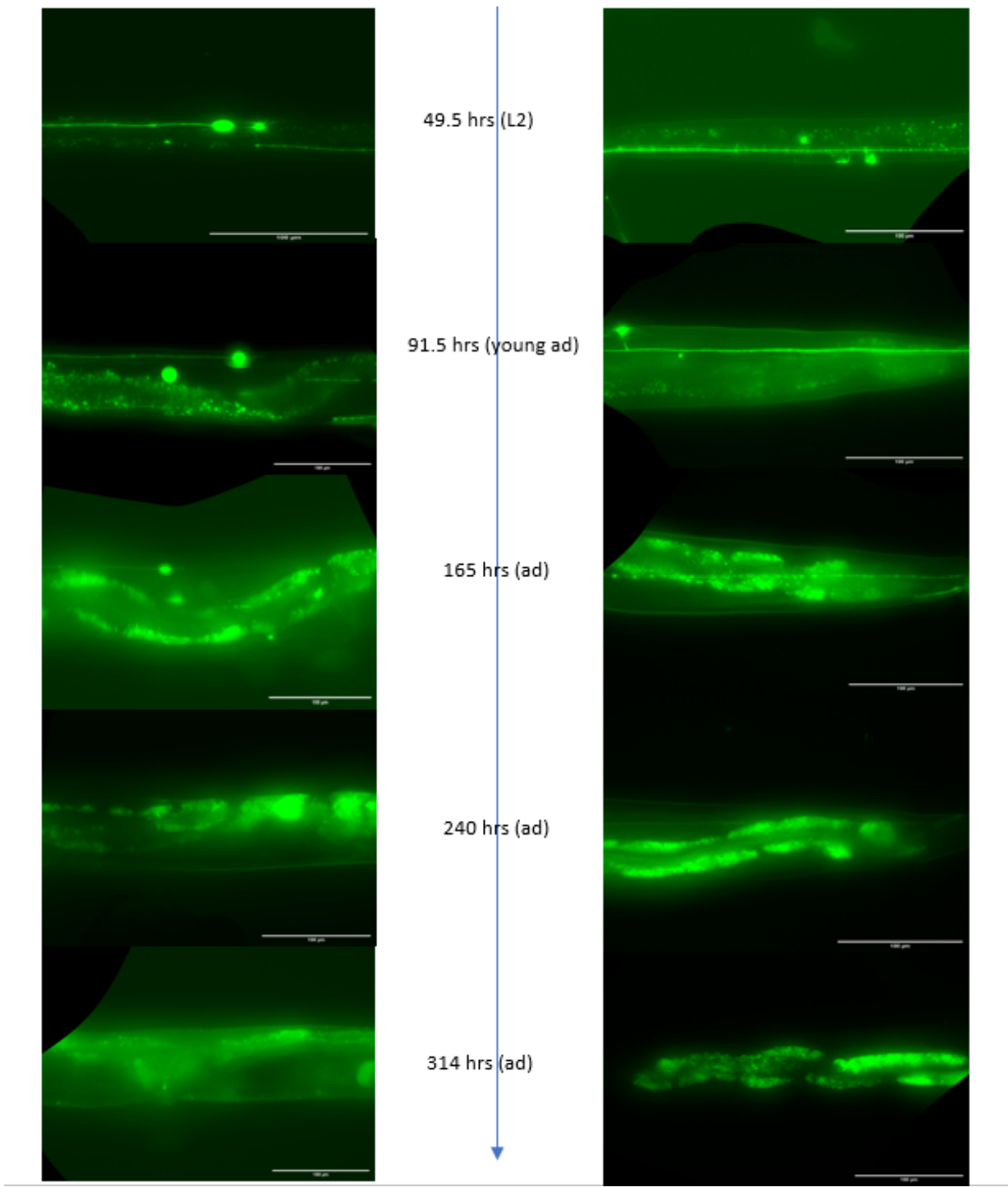


Figure 28: Fluorescence microscopy images of the extrachromosomal strain MSB557 at different ages. The maturity levels are denoted in hours, and using the respective stage's names L2, young adult (young ad) and adult (ad). The left pictures show the anterior neurons in the worms' bodies, whereas the right images depict the posterior neurons in the worms' tails.

The illustrations above depict the increasing autofluorescent blur, as well as the rising intensities of so-called *gut granules*, small circular organelles in gut cells[60]. Consequently, while at young ages, the mNeonGreen-labelled neurons are clearly discernible, these are gradually covered by autofluorescence. One can qualitatively conclude, that the worm's total intensity is progressively increasing, while the neuron-

to-autofluorescence ratio decreases over time, until it reaches zero, when the neuron cannot be identified anymore.

Quantifying the above illustrations, a similar time-chart is depicted using the spatial intensities over the y-axis for each respective image.

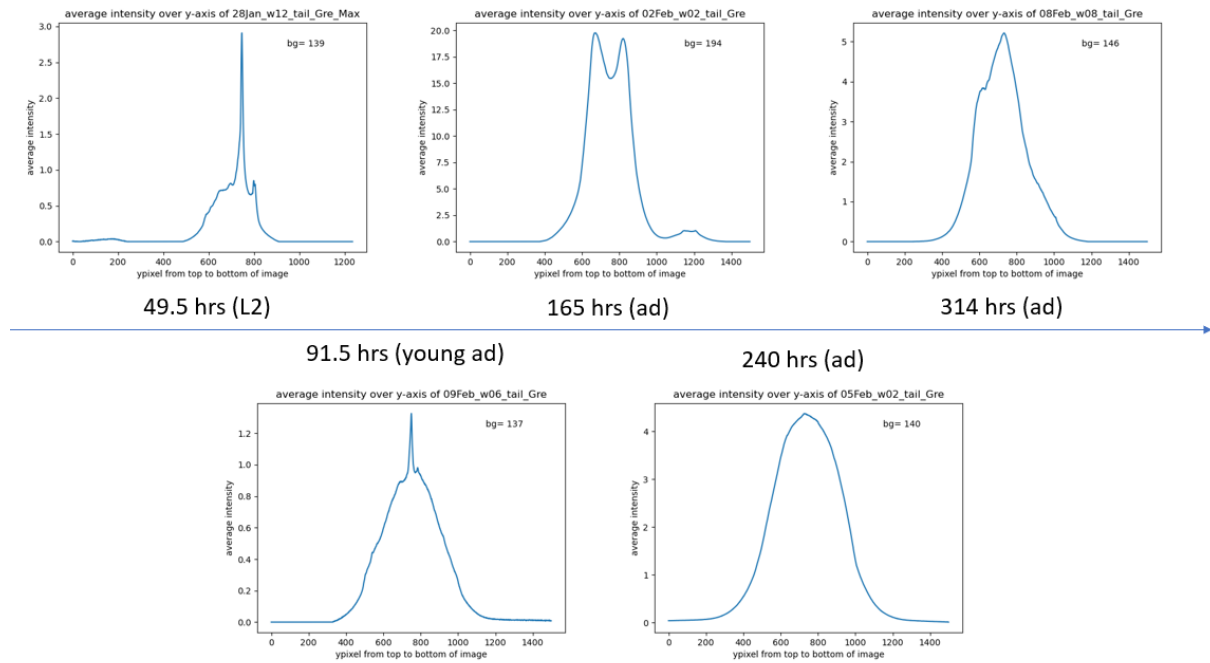


Figure 29: Spatial intensity distributions over the y-axis for each respective fluorescence image of the posterior touch-receptor neurons in the tails.

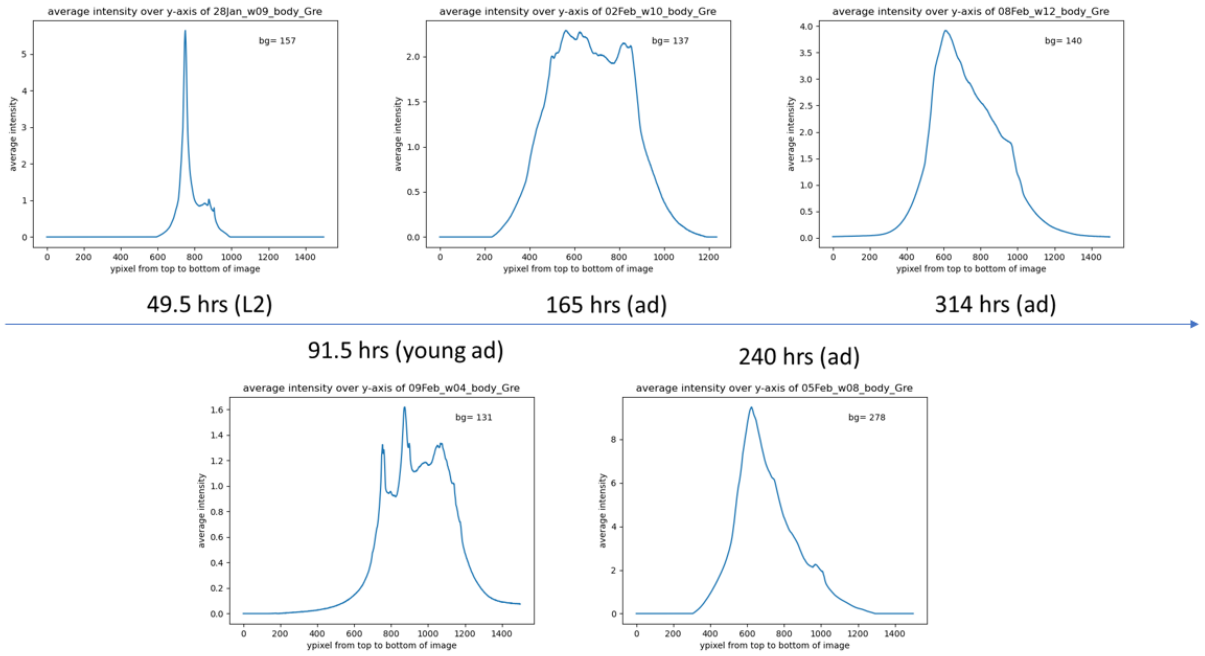


Figure 30: Spatial intensity distributions over the y-axis for each respective fluorescence image of the anterior touch-receptor neurons in the bodies.

According to the above diagrams, similar conclusions are drawn. At young ages, high intensity values are only portrayed by a significant peak, at the neuron's y-coordinate. However, as time passes, intensities increase in the entirety of the worm's width. The denoted peak loses its prominence, and is gradually covered by generally high values. These patterns illustrate the neuron's clear visibility in young worms, due to low autofluorescence in the rest of its body. However, autofluorescence increases over time, until it finally diminishes the neuron's clear visibility.

Qualitative observation of ageing worms, using luminescence microscopy

On the other hand, images taken with the bioluminescence microscope lead do different conclusions. The illustrations below depict different extrachromosomal worms of increasing age. In contrast to fluorescence images, solely neuronal signals are discernible for every stage of development, whereas autofluorescence is not displayed.

Furthermore, this matter is quantitatively observed using the displays of spatial intensities over the the y-axis for the respective images. Regardless of the worm's age, every diagram solely pictures a distinct peak at the neuron's y-coordinate. The remaining width of the worm solely features intensities near the back-ground value. Consequently, the diagrams demonstrate the absence of autofluorescence, and the neuron's clear visibility at every development stage.

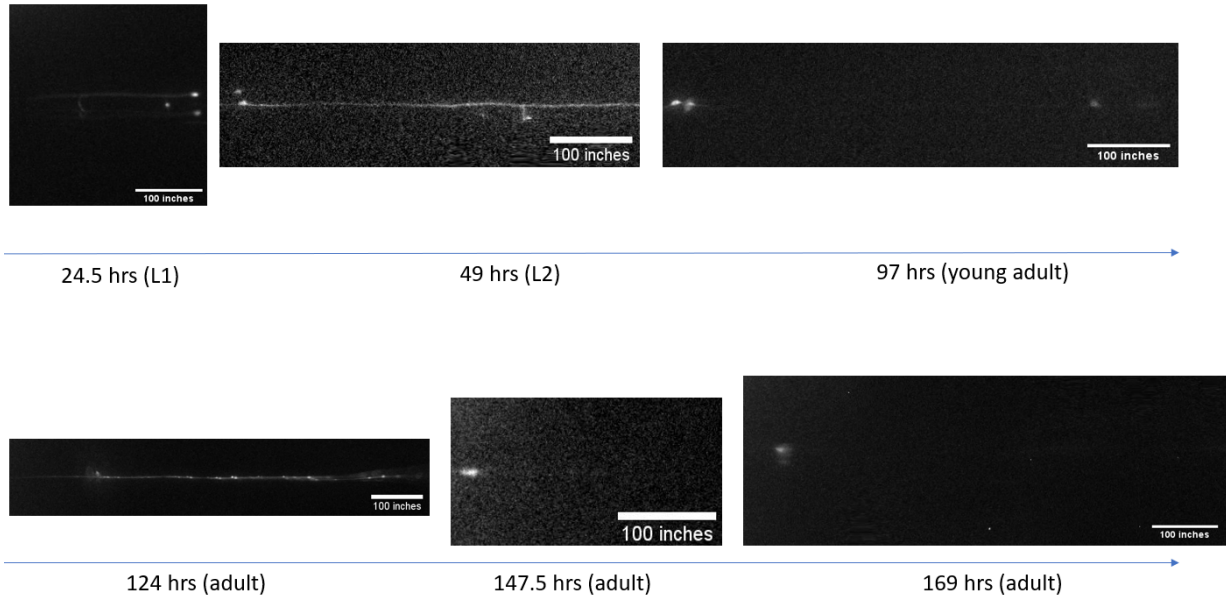


Figure 31: Bioluminescence images of mNeonGreen-labelled neurons in MSB557 for samples of different ages. The maturity is given in hours and the respective stages L1, L2, young adult and adult. (1 inch = 2.54 cm)

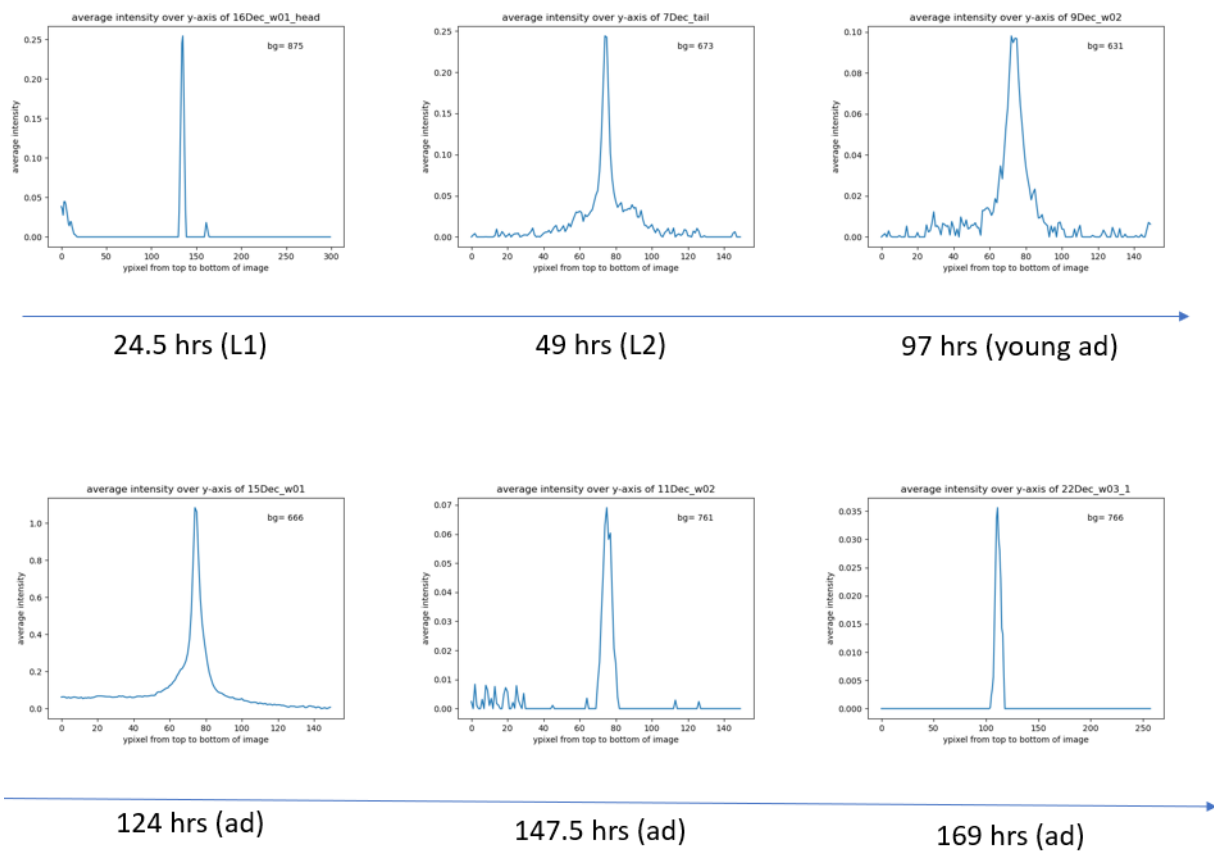


Figure 32: Spatial intensity distributions over the y-axis for the respective bioluminescence images.

4.2 Quantitative evaluation of autofluorescence

Evaluating total intensities

Once qualitative conclusions are drawn, fluorescence microscopy images using the GFP filter-cube are quantitatively evaluated. More precisely, the total intensities of every sample are computed and illustrated in the diagrams below. Each strain is separately assessed. Furthermore, diagrams distinguish between body-areas around the anterior touch-receptor neurons in the tail, and those around posterior touch-receptor neurons near the gonad. On a side note, a jitter has been added to the individual data-points, to make them more discernible. It is not supposed to be interpreted as an age difference between samples.

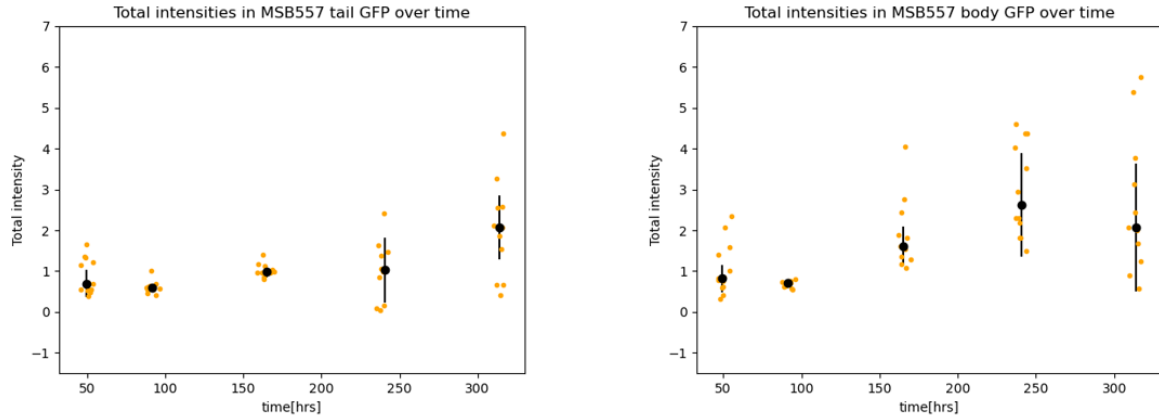


Figure 33: Total intensities of the extrachromosomal strain MSB557 at different ages, using the GFP filter-cube. Individual data-points, as well as medians and median standard deviations are depicted. (right) Intensities in the tails. (left) Intensities in the bodies.

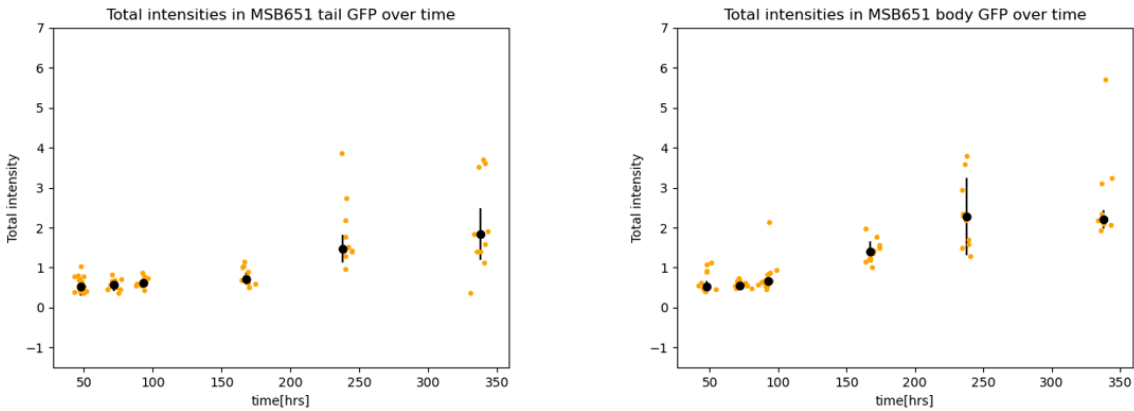


Figure 34: Total intensities of the integrated strain MSB651 at different ages, using the GFP filter-cube. Individual data-points, as well as medians and median standard deviations are depicted. (right) Intensities in the tails. (left) Intensities in the bodies.

Evaluating the above figures, an increase of total intensities for ageing samples, regardless of body-part or strain, is featured. Furthermore, discrepancies between the total intensities of same-aged samples enhance for older worms.

To demonstrate the above patterns, the diagram featuring the total intensities in the bodies of MSB651-samples is studied. For young worms in the L2-stage, values concentrate around ≈ 1 , never outspacing the range between ≈ 0.5 and ≈ 1.3 . On the other hand, their oldest counterparts most commonly display intensities of ≈ 2.5 . Furthermore, their median deviation is significantly higher, represented by a value of ≈ 2 for worms of an age of ≈ 250 hours.

Similar observations are made, when analysing the extrachromosomal strain MSB557. However, especially for older worms, the median deviations feature significantly higher values than those exhibited by the MSB651 strain, regardless of the analysed body-part. Turning the attention back to intensities in the worms' bodies, extrachromosomal samples aged ≈ 250 hours display values in a higher range of ≈ 3.5 than their integrated counterparts.

Lastly, when comparing fluorescence between body-parts, intensities reach higher values in bodies than in tails, especially so, when analysing the extrachromosomal strain. While intensities in the oldest samples' tails reach a maximum value of ≈ 4.5 , they increase until ≈ 6 in the body.

Furthermore, fluorescence microscopy images of the integrated MSB651 strain using the mCherry filter-cube are evaluated in an equal manner. The results are depicted below:

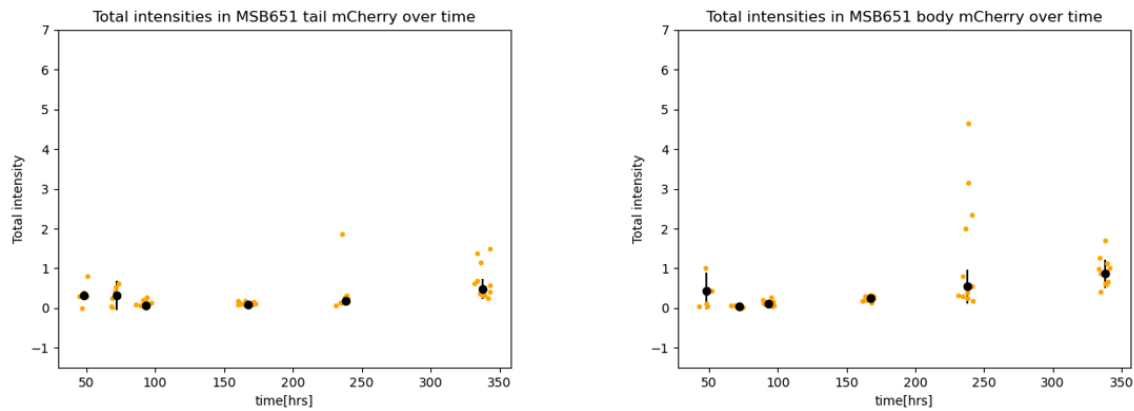


Figure 35: Total intensities of the integrated strain MSB651 at different ages, using the mCherry filter-cube. Individual data-points, as well as medians and median standard deviations are depicted. (right) Intensities in the tails. (left) Intensities in the bodies.

While, in general, the above figures portray similar patterns to their GFP-counterparts, looking more closely reveals meaningful differences. On one hand, the rates of increase and absolute intensity values are not alike for both cubes. Regardless of the sample's age, green fluorescence intensities are always higher and increase more significantly. Turning the attention to intensities in the bodies of MSB651-samples in mCherry-ranges, they feature values close to ≈ 0 for worms until adulthood, while they slightly increase until ≈ 1 for older samples. On the other hand, GFP-wavelengths display intensities close to ≈ 0.5 in the L2-stage, and reach a median value of ≈ 2 for oldest specimens. Similar conclusions can be drawn when comparing the fluorescence in the tails of the samples using both cubes.

On a side note, the above diagram features four outliers in the bodies of ≈ 250 hours aged samples. It has been noticed, that reflections by air bubbles and small cracks in the glass of the microscope slide have a considerable impact on images taken with the mCherry filter-cube. They generate high-intensity spots, which are represented by unexpectedly high values.

Neuron-to-autofluorescence ratios

Lastly, the neuron-to-autofluorescence ratio is a measure, that assesses the development of autofluores-

cence over time, while simultaneously evaluating the signal's visibility. It is portrayed for integrated and extrachromosomal samples, individually analysing their tails and bodies.

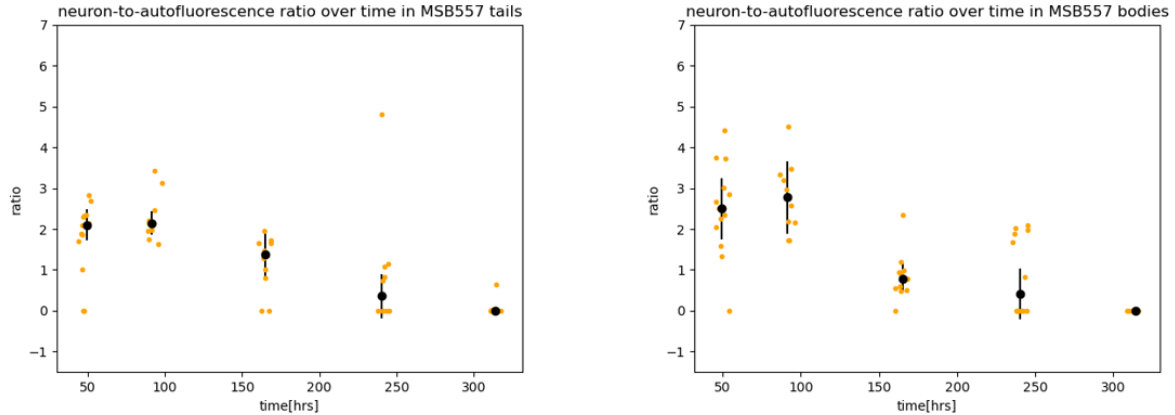


Figure 36: Autofluorescence-to-noise ratios for the extrachromosomal strain MSB557 at different ages. Individual data-points, as well as medians and median standard deviations are depicted. (right) Autofluorescence-to-noise ratios in tails. (left) Autofluorescence-to-noise ratios in bodies.

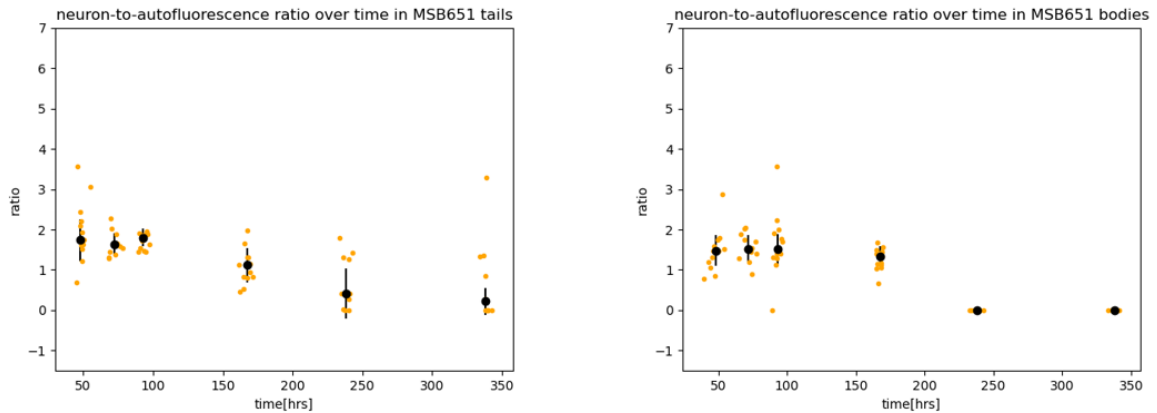


Figure 37: Autofluorescence-to-noise ratios for the integrated strain MSB651 at different ages. Individual data-points, as well as medians and median standard deviations are depicted. (right) Autofluorescence-to-noise ratios in tails. (left) Autofluorescence-to-noise ratios in bodies.

Evaluating the above graphs, the steady decrease of signal-to-autofluorescence ratios until a value of ≈ 0 is most striking. In comparison to the results of total intensities, differences between body-parts and strains are less significant. However, extrachromosomal samples feature higher ratios especially in their bodies, than their integrated counterparts. While young MSB557 worms before adulthood portray values of ≈ 3 , MSB651 ratios gather around ≈ 1.5 .

5 Discussion

Results

Finally, enough insights have been gained to draw a clearer and more detailed picture of the behaviour of autofluorescence in fluorescence and bioluminescence microscopy.

From qualitative observations, it is unambiguous, that autofluorescence is a major drawback in fluorescence microscopy. While worms are young, this phenomenon is not yet significantly developed, allowing the desired signal to be clearly visible. However, with ageing samples autofluorescence increases, until it finally covers the expected signal. Presumably, fluorescence microscopy is only suitable for imaging young samples, and yields a decreasingly satisfying result for older worms.

However, bioluminescence microscopy does not seem to be affected by the above issue. Instead, the signal is visible during the worm's entire life-time. This highlights an important advantage of the denoted imaging technique.

Diving deeper into the characteristics of autofluorescence, it is undoubtedly increasing over age, regardless of strain, wavelength-range or body area. Consequently, it is also known under the names of "age pigment" and "death marker"[61]. Previous studies have shown, that on one hand red and green autofluorescence linearly increase with the worm's ageing, while blue autofluorescence on the other hand peaks shortly before and after death[48]. The specified consistent increase is most probably linked to the accumulation of metabolic byproducts and other compounds over time.

Attempting to determine the denoted autofluorescent materials, a few studies have identified lysosomes in intestinal cells and mitochondria as such[62]. More precisely, they contain increased concentrations of pyridinic (NADPH), flavin coenzymes, as well as *Lipofuscin*, which is known to emit light in the yellow and red wavelengths, after excitation in the blue range[63]. Especially *Lipofuscin* is known as a molecular waste, that accumulates in ageing mammalian cells[64]. Furthermore, *C. elegans* features unfertilised oocytes in its gonad, which contain autofluorescent yolk proteins[48].

While an increase in autofluorescence is observed in all strains, body-parts and wavelength-ranges, its rate differs according to the denoted features. In general, green autofluorescence seems to be more prevalent than its red counterpart, and also rise more significantly in the body than in the tail. According to previous studies, nematodes contain high amounts of lysosome-like *gut granules*[60] in intestinal cells, which are also clearly discernible in the qualitative evaluation. Their exact function is yet only vaguely identified, however, they are suspected to be storage organelles, containing a glycolylated form of *anthranilic acid (AA)*[48]. This compound features especially high fluorescence in the blue emission spectrum, and might be responsible for the predominance of green autofluorescence in the body of *C. elegans*.

In terms of intensity, both strains do not seem to reveal any significant differences. Instead, their dissimilarity lies in the fluctuations between data-points of equally aged specimens. Especially for elderly samples, extrachromosomal animals seem to differ more significantly from each other, than integrated strains. This observation might be rooted in the genetic nature of both strains. As previously outlined, extrachromosomal samples experience an overexpression of the transgenic array, which may have a negative impact on their overall health[40]. As the amount of plasmid-repetitions in the array varies[41], each worm's health is affected differently. Keeping in mind, that autofluorescence is correlated to well-being, discrepancies in extrachromosomal strains might be rooted in the denoted aspects[42]. Furthermore, as these effects increase over time, diversity in autofluorescence becomes more significant in older samples. It must be noted however, that also integrated strains yield higher dissimilarities at advanced ages, although to a less significant extent. In general, this highlights the unpredictability of ageing rates.

Similar conclusions can be drawn from analysing neuron-to-autofluorescence ratios, which also take into account the neuron's intensity and visibility. Again, extrachromosomal strains feature higher signal variability, most probably due to their different genotype. As previously outlined, the extrachromosomal array carries different amounts of mNeonGreen's DNA-sequence. This leads to different extents of expression

amongst siblings of the same strain, and therefore also differing neuronal intensities. Furthermore, the denoted arrays are known to be unevenly transmitted during mitosis. As older specimens have undergone more cell divisions than their younger counterparts, variability increases in ageing worms. The denoted variability in the signal's intensities are coupled with the previously outlined autofluorescence diversity, translating into increased fluctuations of the analysed ratio, especially in older samples[44].

Additionally, regardless of the underlying genetics, autofluorescence is shown to dominate over the signal's intensity for older specimens, more so in the body than in the tail. Most probably, two effects come into play at the same time - on one hand, increasing autofluorescence, but on the other hand, also the downgrade in neuronal health and mNeonGreen-expression. Regardless of transgenesis, *C. elegans* is known to undergo neurodegeneration[65] as time passes, which leads to a signal decrease. It is further impacted by the mentioned decrease in mNeonGreen-expression over time.

Error sources

Theory predicts a clearer and more stable increase in autofluorescence and decrease of autofluorescence-to-noise ratios over time, which is not entirely portrayed by the obtained data. Consequently the experiment is subject to additional constraints, which show effect on the final data presentation. These are evaluated and discussed below.

Turning the attention to the process of imaging, autofluorescence is promoted by increased stress levels of the worms, when they are being mounted. Most probably, some react to a greater extent than others, leading to different autofluorescence intensities. The same argument is also valid while subjecting the worms to laser-light during fluorescence imaging. As the process also causes distress, autofluorescence rises inconsistently amongst the samples.

Other circumstances further increase data variability. On one hand, concentrations of the Agar-pads may not be precisely the same for each imaging process. Furthermore, mounted worms may be surrounded by autofluorescent bacteria. Both issues lead to differing background values, which also alter the quantification of autofluorescence for each sample. On the other hand, photobleaching does not uniformly occur, as worms imaged last have been subjected to high-frequency light for the longest period of time. This is a consequence of mounting all same-age samples on the same pad. It further alters the recorded intensity values. Lastly, scratches on the glass, air bubbles and inconsistent agar-thickness may reflect light in uneven manners, and further falsify the recorded signal. This matter is especially prominent when using the mCherry-setup, as scratches and bubbles seem to reflect higher proportions of light in the denoted wavelength-range.

Still contemplating over the process of imaging, bioluminescence microscopy seems to be accompanied by some difficulties. Most importantly, only few worms feature a measurable signal. Most probably, the Luciferin-substrate is facing difficulties entering the worm's cuticle, and does so in different concentrations. Consequently, signal quality is highly unsteady. Especially older worms feature this issue, possibly additionally as a consequence of decreasing mNeonGreen-expression and neurodegeneration. As a result, an attempt to image worms of 125 hours, as well as 150 hours age did not result in any signal. Furthermore, it is suspected, that the Luciferin-substrate might be unstable, such that it loses its catalytic features during the imaging process. Finally, to further outline inconsistencies of bioluminescence methods, the signal seems to gradually be increasing over time. Consequently, the reaction does not seem to immediately occur at its fullest, and may be subject to other factors.

Now focusing on the method of evaluation, it may also be linked to deviations from the theoretical trend. On one hand, autofluorescence is assessed by means of quantifying the worm's total intensity. This method requires the same neuronal intensity in all samples for relating its increase to the development of autofluorescence. However, in reality, genes are expressed and transcribed to different extents, leading to differing signal strengths. Also the neuron itself is known to degenerate over time.

Still analysing the applied method of evaluation, neuron-to-autofluorescence ratios may be inconsistently studied, as clearly labelling each neuron in acquired images proves to be challenging. Consequently, the term "signal" may be portrayed by different neurons, which possibly express mNeonGreen in various con-

centrations. Furthermore, the neuron-to-autofluorescence ratio is more prone to errors and deviations, than the total intensity, as it is derived by two values subject to inconsistencies - namely the signal strength and the total intensity itself.

6 Summary and Outlook

This research project compares the features of fluorescence and bioluminescence microscopy regarding the disturbing effects of autofluorescence. More precisely, two transgenic strains of *C. elegans* featuring mNeonGreen-labelled touch receptor neurons are imaged and analysed using both microscopy techniques. To outline the role of genetics, extrachromosomal and integrated samples are put into contrast. Furthermore, analysis differentiates between the two spectra of GFP and mCherry, as well as the signals in the worm's tail and body.

Comparing both microscopy techniques showcases their most important difference. While fluorescence relies on external excitation, bioluminescence autonomously initiates a chemical reaction, which sets free the photons to be imaged. This feature disables the numerous disadvantages of fluorescence microscopy, such as photo-bleaching, photo-toxicity, and -of special interest in this project- autofluorescence.

On a first note, signals yielded by both imaging methods are qualitatively compared for different development stages of *C. elegans*. Most strikingly, the steady increase in autofluorescence, when using fluorescence microscopy, is observed. It goes hand in hand with a gradual concealing of the mNeonGreen-labelled touch receptor neurons, until they are fully drowned in the sea of autofluorescence for oldest samples. In contrast, bioluminescence microscopy features visible neurons, regardless of the sample's age. However, images do not always showcase the entire neuron, and at times portray less details than fluorescence methods. This is especially the case for ageing nematodes.

Furthermore, by evaluating the worm's total intensity, the behaviour of autofluorescence is assessed over time, revealing a gradual increase. However, other interesting features are also observed. On one hand, autofluorescence seems to be less prominent and exhibited a lower rate of increase in the tail than in the body. Furthermore, the same conclusion is drawn from comparing signals in the GFP wavelength-range to those in the mCherry range. In the light of literature, both observations are accounted for by identifying fluorescent material in *C. elegans*. Finally, a last interesting feature is portrayed by a higher data-variability in older samples, regardless of the denoted strain. As previous studies have portrayed an existing correlation between health and autofluorescence, data-fluctuations might denote the biological unpredictability of rates of ageing. Furthermore, genetics also plays an important role in terms of health and ageing, as denoted by an amplified data-variability for extrachromosomal strains.

On a final note, the ratios between the neuron's signal and autofluorescence are compared in terms of strain, body-part and wavelength-range. Similar patterns to those mentioned earlier are observed, namely higher data-variability for older specimens, especially extrachromosomal samples, as well as higher ratios in the tail than in the body. Understanding these patterns requires a deeper look in the neuronal signal's development. According to literature, genetics contributes to less stable mNeonGreen-expression and ageing patterns in extrachromosomal samples, as well as general neurodegeneration in both strains.

Having highlighted the different aspects of bioluminescence and fluorescence microscopy, insights are finally solidified. Most importantly, fluorescence microscopy yields a clearly discernible neuronal signal for young worms. However, its suitability decreases over time, suggesting, that bioluminescence might be a preferred method in this case. On top of that, as autofluorescence is more prominent in the body, this matter should be addressed with increased consideration when imaging tissues in the denoted area. Finally, addressing the suitability of different wavelength-ranges in fluorescence microscopy, tissues labelled by mCherry might be better discernible due to lower autofluorescence.

7 Appendix

Python-scripts

Spatial intensity distributions and total intensities over time

```
1 from PIL import Image
2 import numpy as np
3 from matplotlib import pyplot as plt
4 from scipy.optimize import curve_fit
5 from statsmodels import robust
6
7 """
8     insert parameters"""
9 #insert data
10 names_01Feb = ["01Feb_W01_tail_Gre","01Feb_W02_tail_Gre","01Feb_W03_tail_Gre","01
11     Feb_W04_tail_Gre","01Feb_W05_tail_Gre","01Feb_W06_tail_Gre","01Feb_W07_tail_Gre","01
12     Feb_W08_tail_Gre","01Feb_W09_tail_Gre","01Feb_W10_tail_Gre","01Feb_W11_tail_Gre","01
13     Feb_W12_tail_Gre","01Feb_W13_tail_Gre"] #INSERT names of images to be processed
14 names_02Feb = ["02Feb_W01_tail_Gre","02Feb_W02_tail_Gre","02Feb_W03_tail_Gre","02
15     Feb_W04_tail_Gre","02Feb_W05_tail_Gre","02Feb_W06_tail_Gre","02Feb_W07_tail_Gre","02
16     Feb_W08_tail_Gre","02Feb_W09_tail_Gre","02Feb_W10_tail_Gre","02Feb_W11_tail_Gre","02
17     Feb_W12_tail_Gre","02Feb_W13_tail_Gre"] #INSERT names of images to be processed
18 names_04Feb = ["04Feb_W01_tail_Gre","04Feb_W02_tail_Gre","04Feb_W03_tail_Gre","04
19     Feb_W04_tail_Gre","04Feb_W05_tail_Gre","04Feb_W06_tail_Gre","04Feb_W07_tail_Gre","04
20     Feb_W08_tail_Gre","04Feb_W09_tail_Gre","04Feb_W10_tail_Gre","04Feb_W11_tail_Gre","04
21     Feb_W12_tail_Gre","04Feb_W13_tail_Gre"] #INSERT names of images to be processed
22 names_05Feb = ["05Feb_W01_tail_Gre","05Feb_W02_tail_Gre","05Feb_W03_tail_Gre","05
23     Feb_W04_tail_Gre","05Feb_W05_tail_Gre","05Feb_W06_tail_Gre","05Feb_W07_tail_Gre","05
24     Feb_W08_tail_Gre","05Feb_W09_tail_Gre","05Feb_W10_tail_Gre","05Feb_W11_tail_Gre","05
25     Feb_W12_tail_Gre","05Feb_W13_tail_Gre"] #INSERT names of images to be processed
26 names_08Feb = ["08Feb_W01_tail_Gre","08Feb_W02_tail_Gre","08Feb_W03_tail_Gre","08
27     Feb_W04_tail_Gre","08Feb_W05_tail_Gre","08Feb_W06_tail_Gre","08Feb_W07_tail_Gre","08
28     Feb_W08_tail_Gre","08Feb_W09_tail_Gre","08Feb_W10_tail_Gre"] #INSERT names of images to
29     be processed
30 names_12Feb = ["12Feb_W01_tail_Gre","12Feb_W02_tail_Gre","12Feb_W03_tail_Gre","12
31     Feb_W05_tail_Gre","12Feb_W06_tail_Gre","12Feb_W07_tail_Gre","12Feb_W08_tail_Gre","12
32     Feb_W09_tail_Gre","12Feb_W10_tail_Gre","12Feb_W11_tail_Gre","12Feb_W12_tail_Gre"] #
33     INSERT names of images to be processed
34
35 #NO OUTLIERS
36
37 name_sets = [names_01Feb,names_02Feb,names_04Feb,names_05Feb, names_08Feb, names_12Feb] #
38     INSERT aquisition sets
39
40 #enter time of image acquisition
41 time_01Feb = list(np.ones(len(names_01Feb))*72) #INSERT time data
42 time_02Feb = list(np.ones(len(names_02Feb))*93) #INSERT time data
43 time_04Feb = list(np.ones(len(names_04Feb))*48) #INSERT time data
44 time_05Feb = list(np.ones(len(names_05Feb))*167.5) #INSERT time data
45 time_08Feb = list(np.ones(len(names_08Feb))*238) #INSERT time data
46 time_12Feb = list(np.ones(len(names_12Feb))*338) #INSERT time data
47
48
49 time_sets = [time_01Feb,time_02Feb,time_04Feb,time_05Feb, time_08Feb, time_12Feb] #INSERT
50     acquisition times-sets
51
52 """
53     Prepare time and names list for processing"""
54
55 ##add times to single list
56 time_01Feb = [str(t) for t in time_01Feb] #INSERT acquisition set
57 time_02Feb = [str(t) for t in time_02Feb] #INSERT acquisition set
58 time_04Feb = [str(t) for t in time_04Feb] #INSERT acquisition set
59 time_05Feb = [str(t) for t in time_05Feb] #INSERT acquisition set
60 time_08Feb = [str(t) for t in time_08Feb] #INSERT acquisition set
61 time_12Feb = [str(t) for t in time_12Feb] #INSERT acquisition set
```

```

43
44
45
46 time = time_01Feb + time_02Feb + time_04Feb + time_05Feb + time_08Feb + time_12Feb #INSERT
    acuisition set time+time+...
47
48 #convert elements back into floats
49 time = [np.float(t) for t in time]
50
51 """y spatial intensity distribution"""
52 #Plot intensity profiles?
53 plot_y_inten=False
54 fig_y_inten_distr = 1
55 #Plot intensity profiles in same graph?
56 same_graph_y = False #If false, graphs are plotted individually
57
58 """Gaussian fit for background and worm position"""
59 #Plot Gaussian on y spatial intensity distribution?
60 plotgauss= False
61
62 """x spatial intensity distribution"""
63 #Plot intensity profiles?
64 plot_x_inten=False
65 fig_x_inten_distr = 2
66 #Plot intensity profiles in same graph?
67 same_graph_x = False #If false, graphs are plotted individually
68
69
70 """total intensity over time"""
71 #Plot each data point?
72 plot_points = True
73 fig_tot_inten_points = 3
74 #Plot statistics?
75 plot_stats= True
76 fig_tot_inten_stats = 4
77 #Plot both in same graph?
78 plot_both = True
79 fig_tot_inten = 5
80
81
82 """Processing function"""
83 def process(imname,index_acquisitionset):
84     """open image"""
85     im = Image.open(imname+".tif")
86     #im.show()
87     impixels=np.array(im)
88
89     """basic facts"""
90     #get shape of picture
91     #eg [[1,2,3],[4,5,6]] is (2,3)
92     xsize= int(impixels.shape[1])
93     ysize= int(impixels.shape[0])
94     print("xsize", xsize, "ysize",ysize)
95
96     #get pixel-type
97     print("type", impixels.dtype)
98     #eg float32 floating point number ranging from -3.39x1038 to +3.39x1038
99
100    #maximum pixel-value
101    print("maximum", np.max(impixels))
102
103    #minimum pixel-value
104    print("minimum", np.min(impixels))
105
106    """get columns"""
107    columns= []
108    #set the amount of lines by defining stepsize in range(0,xsize, xsize/XXX)
109    for i in range(0,xsize):
110        columns.append(impixels[:,i])
111

```

```

112     columns=np.array(columns)
113
114     #columns.shape yields (x,y) means I have x columns of a length of y
115     amount_columns = int(columns.shape[0]) #lines earlier
116     length_columns = int(columns.shape[1]) #length earlier
117     print("amount of columns", amount_columns)
118     print("length of columns", length_columns)
119     #[[1 2 3 4] [1 2 3 4]] is columns with 2 lines of length 4
120
121
122     """calculating background"""
123     ##ignore columns with black spots due to straightening
124
125     #create new columns-list
126     x = []
127
128     #check if line contains 0 value, and delete line if so
129     for i in range(0,amount_columns):
130         for j in range(0,length_columns):
131             if columns[i,j] == 0:
132                 break
133             elif j == length_columns - 1:
134                 x.append(columns[i])
135             else:
136                 continue
137     cropped_columns = np.array(x)
138
139     #dimensions of cropped picture:
140     cropped_amount_columns = int(cropped_columns.shape[0])
141     length_columns = int(cropped_columns.shape[1])
142     #print("cropped amount of columns", amount_columns)
143     #[[1 2 3 4] [1 2 3 4]] is columns with 2 lines of length 4
144
145
146     ##Average over all columns
147
148     #summing pixels of every column
149     sum = [] # gives single column with sum of all lines
150     for j in range(0,length_columns):
151         x = cropped_columns[0,j]
152         for i in range(1,cropped_amount_columns-1):
153             x = x + cropped_columns[i,j]
154         sum.append(x)
155
156     sum = np.array(sum)
157
158     #dividing by amount of lines
159     cropped_avercolumn = sum/cropped_amount_columns
160     #print("average line", averline)
161
162     ##Gaussian fit on intensity distribution
163     #intensity data
164     x = np.arange(0,length_columns)
165     y = cropped_avercolumn
166
167     #fitting function and parameters
168     def Gauss(x,a,x0,sigma,c):
169         return a*np.exp(-(x-x0)**2/(2*sigma**2))+c
170
171     a = np.max(y)
172     x0=length_columns/2
173     sigma = 100
174     c = np.min(y)
175
176     popt,pcov = curve_fit(Gauss, x, y, p0=[a, x0, sigma, c])
177
178     #Plotting
179     if plotgauss == True:
180         plt.figure()
181         plt.plot(x, y, 'b-', label='aver y-inten')

```

```

182     plt.plot(x,Gauss(x, *popt), 'r-', label='fit')
183     plt.legend()
184     plt.title('Fit of worm position')
185     plt.xlabel('height of image from top to bottom')
186     plt.ylabel('Intensity')
187     plt.savefig(str(imname)+"_average_intensity_gaussian")
188     plt.close()
189 else:
190     pass
191
192 ##determine background as Gauss-baseline
193 bg = popt[3]
194
195 """Setting black spots to background value"""
196 #check if line contains 0 value
197 for i in range(0,amount_columns):
198     for j in range(0,length_columns):
199         if columns[i,j] == 0:
200             columns[i,j] = bg
201
202
203 """Average over all columns"""
204 #summing pixels of every column
205 sum = [] # gives single column with sum of all lines
206 for j in range(0,length_columns):
207     x = columns[0,j]
208     for i in range(1,amount_columns-1):
209         x = x + columns[i,j]
210     sum.append(x)
211
212 sum = np.array(sum)
213
214 #dividing by amount of columns
215 avercolumn = sum/amount_columns
216 #print("averaged column", avercolumn)
217
218
219 """background subtraction"""
220 avercolumn = (avercolumn - bg)/bg
221
222 #set negative pixels to zero
223 for i in range(0,length_columns):
224     if avercolumn[i]<0:
225         avercolumn[i]=0
226
227 """Illustration of spatial intensity distribution in y"""
228 if plot_y_inten==True:
229
230     if same_graph_y == True:
231         plt.figure(fig_y_inten_distr)
232         x = np.arange(0,length_columns)
233         y = avercolumn
234         plt.plot(x,y,label=imname[6:9]+" bg= "+str(int(bg)))
235         plt.xlabel("ypixel from top to bottom of image")
236         plt.ylabel("average intensity")
237         plt.title("average intensity over y-axis for "+imname[0:5]+imname[9:22])
238         plt.legend()
239         plt.savefig("y_intensity_distribution"+imname[0:4]+imname[9:22])
240         if imname == name_sets[index_acquisitionset][-1]:
241             plt.close(fig_y_inten_distr)
242         else:
243             pass
244
245     else:
246         fig = plt.figure()
247         x = np.arange(0,length_columns)
248         y = avercolumn
249         plt.plot(x,y,label=imname[6:8])
250         plt.xlabel("ypixel from top to bottom of image")
251         plt.ylabel("average intensity")

```

```

252         plt.title("average intensity over y-axis of "+imname)
253         plt.figtext(.7, .8, "bg= "+str(int(bg)))
254         plt.savefig(str(imname)+"_y_intensity_distribution")
255         plt.close (fig)
256
257     else:
258         pass
259
260
261     """Illustration of spatial intensity distribution in x"""
262     ##get lines
263     lines= []
264     #set the amount of lines by defining stepsize in range(0,xsize, xsize/XXX)
265     for i in range(0,ysize):
266         lines.append(impixels[i,:])
267
268     lines=np.array(lines)
269
270     #lines.shape yields (x,y) means I have x lines of a length of y
271     amount_lines = int(lines.shape[0])
272     length_lines = int(lines.shape[1])
273     print("amount of lines", amount_lines)
274     print("length of lines", length_lines)
275     #[[1 2 3 4] [1 2 3 4]] is 2 lines of length 4
276
277
278     ##cropping lines to those that contain worm: [x0-3sigma, x0+3sigma]
279     lines = lines[int(popt[1]-3*popt[2]):int(popt[1]+popt[2])]
280     amount_lines = int(lines.shape[0])
281     length_lines = int(lines.shape[1])
282
283     ##Average over all lines
284
285     #summing pixels of every line
286     sum = [] # gives single line with sum of all lines
287     for j in range(0,length_lines):
288         x = lines[0,j]
289         for i in range(1,amount_lines-1):
290             x = x + lines[i,j]
291         sum.append(x)
292
293     sum = np.array(sum)
294
295     #dividing by amount of lines
296     averline = sum/amount_lines
297     #print("average line", averline)
298
299     ##background subtraction
300     averline = (averline - bg)/bg
301
302     #set negative pixels to zero
303     for i in range(0,length_lines):
304         if averline[i]<0:
305             averline[i]=0
306
307     ##Illustration of spatial intensity distribution in x"""
308     if plot_x_inten==True:
309
310         if same_graph_x == True:
311             plt.figure(fig_x_inten_distr)
312             x = np.arange(0,length_lines)
313             y = averline
314             plt.plot(x,y,label=imname[6:9]+" bg= "+str(int(bg)))
315             plt.xlabel("xpixel from left to right")
316             plt.ylabel("average intensity")
317             plt.title("average intensity over x-axis for "+imname[0:5]+imname[9:22])
318             plt.legend()
319             plt.savefig("x_intensity_distribution"+imname[0:4]+imname[9:22])
320             if imname == name_sets[index_acquisitionset][-1]:
321                 plt.close(fig_x_inten_distr)

```

```

322         else:
323             pass
324
325     else:
326         fig = plt.figure()
327         x = np.arange(length_lines)
328         y = averline
329         plt.plot(x,y,label=imname[6:8])
330         plt.xlabel("xpixel from left to right")
331         plt.ylabel("average intensity")
332         plt.title("average intensity over x-axis of "+imname)
333         plt.figtext(.7, .8, "bg= "+str(int(bg)))
334         plt.savefig(str(imname)+"_x_intensity_distribution")
335         plt.close (fig)
336
337     else:
338         pass
339
340
341     """Averaging total intensity of picture"""
342     #cropping averaged column to y-pixels that contain worm: [x0-3sigma, x0+3sigma]
343     x = avercolumn[int(popt[1]-3*popt[2]):int(popt[1]+popt[2])]
344     #calculating total intensity value per area: Sum of all intensity values divided width
345     #of the worm
346     tot_inten_value = np.sum(x)/(float(len(x)))
347     #appending to list for later processing
348     totintensity.append(tot_inten_value)
349     calc_stats.append(tot_inten_value)
350
351 """
352 name_sets=np.array(name_sets,dtype=object)
353
354 totintensity = [] #list of total intensity values for each image
355 stats_acquisitions = [] #list of statistical values for each acquisition set
356 calc_stats = [] #list for calculating statistical values of each acquisition set
357
358 for index_acquisitionset in range(0,len(name_sets)): #loop through acquisition sets
359     print("Set of " + str(name_sets[index_acquisitionset][1][0:6])+str(name_sets[
360         index_acquisitionset][1][10:22]))
361     for j in range(0,len(name_sets[index_acquisitionset])): #loop through images of one set
362         imname= name_sets[index_acquisitionset][j]
363         print("image", imname)
364
365         process(imname,index_acquisitionset) #add tot_inten_value to totintensity-list for
366         #chosen image
367
368         ##if last image of set reached, determine statistics: stats_acquisitions=[median_set1,median_dev_set1, med_set2,med_dev_set2,...]
369         if imname == name_sets[index_acquisitionset][-1]:
370             median = np.median(calc_stats_sn)
371             print("Median=",median)
372             stats_acquisitions_sn.append(median)
373             mean = np.mean(calc_stats_sn)
374             print("Mean=",mean)
375             std = np.std(calc_stats_sn)
376             print("std=",std)
377             meddev = robust.mad(calc_stats_sn)
378             stats_acquisitions_sn.append(meddev)
379
380             calc_stats = [] #after acquisition set fully processed, clear data
381         else:
382             pass
383
384 """
385 if plot_stats== True:
386     #median values
387     means=np.array(stats_acquisitions [0:len(stats_acquisitions):2])
388     #median deviations as errors
389     std=np.array(stats_acquisitions [1:len(stats_acquisitions):2])

```

```

388     #time points
389     t = []
390     for i in range(0,len(time_sets)):
391         t.append(float(time_sets[i][0])) #append first time point for each acquisition set
392     t=np.array(t)
393
394     ##plot figure
395     plt.figure(fig_tot_inten_stats)
396     plt.errorbar(t, means, std, linestyle='None', marker='x')
397     plt.xlabel("time[hrs]")
398     plt.ylabel("total intensity")
399     plt.title("total intensity of over time")
400     plt.savefig("total_intensity_over_time_stats_"+imname[0:6]+imname[10:22])
401     plt.close(fig_tot_inten_stats)
402 else:
403     pass
404
405 """Plotting total intensity over time"""
406 if plot_points==True:
407     plt.figure(fig_tot_inten_points)
408     totintensity = np.array(totintensity)
409     plt.errorbar(time,totintensity,linestyle='None', marker='x')
410
411     plt.xlabel("time[hrs]")
412     plt.ylabel("total intensity")
413     plt.title("total intensity of over time")
414     plt.savefig("total_intensity_over_time_points_"+imname[0:6]+imname[10:22])
415     plt.close(fig_tot_inten_points)
416 else:
417     pass
418
419 if plot_both == True:
420
421     plt.figure(fig_tot_inten)
422
423     ##prepare data
424     #median values
425     means=np.array(stats_acquisitions[0:len(stats_acquisitions):2])
426     #median deviations as errors
427     std=np.array(stats_acquisitions[1:len(stats_acquisitions):2])
428     #time points
429     t = []
430     for i in range(0,len(time_sets)):
431         t.append(time_sets[i][0]) #append first time point for each acquisition set
432     t=np.array(t)
433
434     totintensity = np.array(totintensity)
435
436     ##plot both graphs
437     plt.subplot(2,1,1)
438     plt.errorbar(time,totintensity,linestyle='None', marker='x')
439     plt.ylabel("total intensity")
440     plt.title("total intensity of over time")
441
442     plt.subplot(2, 1, 2)
443     plt.errorbar(t, means, std, linestyle='None', marker='x')
444     plt.xlabel("time[hrs]")
445     plt.ylabel("total intensity")
446
447     plt.savefig("total_intensity_over_time_"+imname[0:6]+imname[10:22])
448     plt.close(fig_tot_inten)

```

Script to determine autofluorescence-to-noise ratios

```
1  from PIL import Image
2  import numpy as np
3  from matplotlib import pyplot as plt
4  from scipy.optimize import curve_fit
5  from statsmodels import robust
6
7
8  """insert parameters"""
9  #insert data
10 names_01Feb = ["01Feb_W01_tail_Gre", "01Feb_W02_tail_Gre", "01Feb_W03_tail_Gre", "01
    Feb_W04_tail_Gre", "01Feb_W05_tail_Gre", "01Feb_W06_tail_Gre", "01Feb_W07_tail_Gre", "01
    Feb_W08_tail_Gre", "01Feb_W09_tail_Gre", "01Feb_W10_tail_Gre", "01Feb_W11_tail_Gre", "01
    Feb_W12_tail_Gre", "01Feb_W13_tail_Gre"] #INSERT names of images to be processed
11 neurons_01Feb = ["01Feb_N01_tail_Gre", "01Feb_N02_tail_Gre", "01Feb_N03_tail_Gre", "01
    Feb_N04_tail_Gre", "01Feb_N05_tail_Gre", "01Feb_N06_tail_Gre", "01Feb_N07_tail_Gre", "01
    Feb_N08_tail_Gre", "01Feb_N09_tail_Gre", "01Feb_N10_tail_Gre", "01Feb_N11_tail_Gre", "01
    Feb_N12_tail_Gre", "01Feb_N13_tail_Gre"]
12
13 names_02Feb = ["02Feb_W01_tail_Gre", "02Feb_W02_tail_Gre", "02Feb_W03_tail_Gre", "02
    Feb_W04_tail_Gre", "02Feb_W05_tail_Gre", "02Feb_W06_tail_Gre", "02Feb_W07_tail_Gre", "02
    Feb_W08_tail_Gre", "02Feb_W09_tail_Gre", "02Feb_W10_tail_Gre", "02Feb_W11_tail_Gre", "02
    Feb_W12_tail_Gre", "02Feb_W13_tail_Gre"] #INSERT names of images to be processed
14 neurons_02Feb = ["02Feb_N01_tail_Gre", "02Feb_N02_tail_Gre", "02Feb_N03_tail_Gre", "02
    Feb_N04_tail_Gre", "02Feb_N05_tail_Gre", "02Feb_N06_tail_Gre", "02Feb_N07_tail_Gre", "02
    Feb_N08_tail_Gre", "02Feb_N09_tail_Gre", "02Feb_N10_tail_Gre", "02Feb_N11_tail_Gre", "02
    Feb_N12_tail_Gre", "02Feb_N13_tail_Gre"]
15
16 names_04Feb = ["04Feb_W01_tail_Gre", "04Feb_W02_tail_Gre", "04Feb_W03_tail_Gre", "04
    Feb_W04_tail_Gre", "04Feb_W05_tail_Gre", "04Feb_W06_tail_Gre", "04Feb_W07_tail_Gre", "04
    Feb_W08_tail_Gre", "04Feb_W09_tail_Gre", "04Feb_W10_tail_Gre", "04Feb_W11_tail_Gre", "04
    Feb_W12_tail_Gre", "04Feb_W13_tail_Gre"] #INSERT names of images to be processed
17 neurons_04Feb = ["04Feb_N01_tail_Gre", "04Feb_N02_tail_Gre", "04Feb_N03_tail_Gre", "04
    Feb_N04_tail_Gre", "04Feb_N05_tail_Gre", "04Feb_N06_tail_Gre", "04Feb_N07_tail_Gre", "04
    Feb_N08_tail_Gre", "04Feb_N09_tail_Gre", "04Feb_N10_tail_Gre", "04Feb_N11_tail_Gre", "04
    Feb_N12_tail_Gre", "04Feb_N13_tail_Gre"]
18
19 names_05Feb = ["05Feb_W01_tail_Gre", "05Feb_W02_tail_Gre", "05Feb_W03_tail_Gre", "05
    Feb_W04_tail_Gre", "05Feb_W05_tail_Gre", "05Feb_W06_tail_Gre", "05Feb_W07_tail_Gre", "05
    Feb_W08_tail_Gre", "05Feb_W09_tail_Gre", "05Feb_W10_tail_Gre", "05Feb_W11_tail_Gre", "05
    Feb_W12_tail_Gre", "05Feb_W13_tail_Gre"] #INSERT names of images to be processed
20 neurons_05Feb = ["05Feb_N01_tail_Gre", "05Feb_N02_tail_Gre", "05Feb_N03_tail_Gre", "05
    Feb_N04_tail_Gre", "05Feb_N05_tail_Gre", "05Feb_N06_tail_Gre", "05Feb_N07_tail_Gre", "05
    Feb_N08_tail_Gre", "05Feb_N09_tail_Gre", "05Feb_N10_tail_Gre", "05Feb_N11_tail_Gre", "05
    Feb_N12_tail_Gre", "05Feb_N13_tail_Gre"]
21
22 names_08Feb = ["08Feb_W01_tail_Gre", "08Feb_W02_tail_Gre", "08Feb_W03_tail_Gre", "08
    Feb_W04_tail_Gre", "08Feb_W05_tail_Gre", "08Feb_W06_tail_Gre", "08Feb_W07_tail_Gre", "08
    Feb_W08_tail_Gre", "08Feb_W09_tail_Gre", "08Feb_W10_tail_Gre"] #INSERT names of images to
    be processed
23 neurons_08Feb = ["08Feb_N01_tail_Gre", "08Feb_N02_tail_Gre", "08Feb_N03_tail_Gre", "08
    Feb_N04_tail_Gre", "08Feb_N05_tail_Gre", "08Feb_N06_tail_Gre", "08Feb_N07_tail_Gre", "08
    Feb_N08_tail_Gre", "08Feb_N09_tail_Gre", "08Feb_N10_tail_Gre"]
24
25 names_12Feb = ["12Feb_W01_tail_Gre", "12Feb_W02_tail_Gre", "12Feb_W03_tail_Gre", "12
    Feb_W05_tail_Gre", "12Feb_W06_tail_Gre", "12Feb_W07_tail_Gre", "12Feb_W08_tail_Gre", "12
    Feb_W09_tail_Gre", "12Feb_W10_tail_Gre", "12Feb_W11_tail_Gre", "12Feb_W12_tail_Gre"] #
    INSERT names of images to be processed
26 neurons_12Feb = ["12Feb_N01_tail_Gre", "12Feb_N02_tail_Gre", "12Feb_N03_tail_Gre", "12
    Feb_N05_tail_Gre", "12Feb_N06_tail_Gre", "12Feb_N07_tail_Gre", "12Feb_N08_tail_Gre", "12
    Feb_N09_tail_Gre", "12Feb_N10_tail_Gre", "12Feb_N11_tail_Gre", "12Feb_N12_tail_Gre"]
27
28
29 #NO OUTLIERS
30
31 name_sets = [names_01Feb, neurons_01Feb, names_02Feb, neurons_02Feb, names_04Feb, neurons_04Feb,
    names_05Feb, neurons_05Feb, names_08Feb, neurons_08Feb, names_12Feb, neurons_12Feb] #INSERT
```

```

    aquisition sets
32
33 #enter time of image acquisition
34 time_01Feb = list(np.ones(len(names_01Feb))*72) #INSERT time data
35 time_02Feb = list(np.ones(len(names_02Feb))*93) #INSERT time data
36 time_04Feb = list(np.ones(len(names_04Feb))*48) #INSERT time data
37 time_05Feb = list(np.ones(len(names_05Feb))*167.5) #INSERT time data
38 time_08Feb = list(np.ones(len(names_08Feb))*238) #INSERT time data
39 time_12Feb = list(np.ones(len(names_12Feb))*338) #INSERT time data
40
41
42
43 time_sets = [time_01Feb,time_02Feb,time_04Feb,time_05Feb, time_08Feb, time_12Feb] #INSERT
    acquisition times-sets
44
45 """Prepare time and names list for processing"""
46
47 ##add times to single list
48 time_01Feb = [str(t) for t in time_01Feb] #INSERT acquisition set
49 time_02Feb = [str(t) for t in time_02Feb] #INSERT acquisition set
50 time_04Feb = [str(t) for t in time_04Feb] #INSERT acquisition set
51 time_05Feb = [str(t) for t in time_05Feb] #INSERT acquisition set
52 time_08Feb = [str(t) for t in time_08Feb] #INSERT acquisition set
53 time_12Feb = [str(t) for t in time_12Feb] #INSERT acquisition set
54
55
56
57 time = time_01Feb + time_02Feb + time_04Feb + time_05Feb + time_08Feb + time_12Feb #INSERT
    acuisition set time+time+...
58
59 #convert elements back into floats
60 time = [np.float(t) for t in time]
61
62 """y spatial intensity distribution"""
63 #Plot intensity profiles?
64 plot_y_inten=False
65 fig_y_inten_distr = 1
66 #Plot intensity profiles in same graph?
67 same_graph_y = False #If false, graphs are plotted individually
68
69 """Gaussian fit for background and worm position"""
70 #Plot Gaussian on y spatial intensity distribution?
71 plotgauss= False
72
73
74 """total intensity over time"""
75 #Plot each data point?
76 plot_points = True
77 fig_snratio_points = 3
78 #Plot statistics?
79 plot_stats= True
80 fig_snratio_stats = 4
81 #Plot both in same graph?
82 plot_both = True
83 fig_snratio = 5
84
85
86 """Processing function"""
87 def process(imname,imname_n, index_acquisitionset):
88     """open image"""
89     im = Image.open(imname+".tif")
90     #im.show()
91     impixels=np.array(im)
92
93     """basic facts"""
94     #get shape of picture
95     #eg [[1,2,3],[4,5,6]] is (2,3)
96     xsize= int(impixels.shape[1])
97     ysize= int(impixels.shape[0])
98     print("xsize", xsize, "ysize",ysize)

```

```

99
100 #get pixel-type
101 print("type", impixels.dtype)
102 #eg float32 floating point number ranging from -3.39x1038 to +3.39x1038
103
104 #maximum pixel-value
105 print("maximum", np.max(impixels))
106
107 #minimum pixel-value
108 print("minimum", np.min(impixels))
109
110 """get columns"""
111 columns= []
112 #set the amount of lines by defining stepsize in range(0,xsize, xsizexXXX)
113 for i in range(0,xsize):
114     columns.append(impixels[:,i])
115
116 columns=np.array(columns)
117
118 #columns.shape yields (x,y) means I have x columns of a length of y
119 amount_columns = int(columns.shape[0]) #lines earlier
120 length_columns = int(columns.shape[1]) #length earlier
121 print("amount of columns", amount_columns)
122 print("length of columns", length_columns)
123 #[[1 2 3 4] [1 2 3 4]] is columns with 2 lines of length 4
124
125
126 """calculating background"""
127 ##ignore columns with black spots due to straightening
128
129 #create new columns-list
130 x = []
131
132 #check if line contains 0 value, and delete line if so
133 for i in range(0,amount_columns):
134     for j in range(0,length_columns):
135         if columns[i,j] == 0:
136             break
137         elif j == length_columns -1:
138             x.append(columns[i])
139         else:
140             continue
141 cropped_columns = np.array(x)
142
143 #dimensions of cropped picture:
144 cropped_amount_columns = int(cropped_columns.shape[0])
145 length_columns = int(cropped_columns.shape[1])
146 #print("cropped amount of columns", amount_columns)
147 #[[1 2 3 4] [1 2 3 4]] is columns with 2 lines of length 4
148
149
150 ##Average over all columns
151
152 #summing pixels of every column
153 sum = [] # gives single column with sum of all lines
154 for j in range(0,length_columns):
155     x = cropped_columns[0,j]
156     for i in range(1,cropped_amount_columns-1):
157         x = x + cropped_columns[i,j]
158     sum.append(x)
159
160 sum = np.array(sum)
161
162 #dividing by amount of lines
163 cropped_avercolumn = sum/cropped_amount_columns
164 #print("average line", averline)
165
166 ##Gaussian fit on intensity distribution
167 #intensity data
168 x = np.arange(0,length_columns)

```

```

169     y = cropped_avercolumn
170
171     #fitting function and parameters
172     def Gauss(x,a,x0,sigma,c):
173         return a*np.exp(-(x-x0)**2/(2*sigma**2))+c
174
175     a = np.max(y)
176     x0=length_columns/2
177     sigma = 100
178     c = np.min(y)
179
180     popt,pcov = curve_fit(Gauss, x, y, p0=[a, x0, sigma, c])
181
182     #Plotting
183     if plotgauss == True:
184         plt.figure()
185         plt.plot(x, y, 'b-', label='aver y-inten')
186         plt.plot(x,Gauss(x, *popt), 'r-', label='fit')
187         plt.legend()
188         plt.title('Fit of worm position')
189         plt.xlabel('height of image from top to bottom')
190         plt.ylabel('Intensity')
191         plt.savefig(str(imname)+"_average_intensity_gaussian")
192         plt.close()
193     else:
194         pass
195
196     ##determine backrgound as Gauss-baseline
197     bg = popt[3]
198
199     """Setting black spots to background value"""
200     #check if line contains 0 value
201     for i in range(0,amount_columns):
202         for j in range(0,length_columns):
203             if columns[i,j] == 0:
204                 columns[i,j] = bg
205
206     """Average over all columns"""
207     #summing pixels of every column
208     sum = [] # gives single column with sum of all lines
209     for j in range(0,length_columns):
210         x = columns[0,j]
211         for i in range(1,amount_columns-1):
212             x = x + columns[i,j]
213         sum.append(x)
214
215     sum = np.array(sum)
216
217     #dividing by amount of columns
218     avercolumn = sum/amount_columns
219     #print("averaged column", avercolumn)
220
221
222     """background subtraction"""
223     avercolumn = (avercolumn - bg)/bg
224
225     #set negative pixels to zero
226     for i in range(0,length_columns):
227         if avercolumn[i]<0:
228             avercolumn[i]=0
229
230     """Process total intensity of neurons"""
231     ##load neuron
232     im_n = Image.open(imname_n+".tif")
233     impixels_n = np.array(im_n)
234
235     ##details
236     xsize_n = int(impixels_n.shape[1])
237     ysize_n = int(impixels_n.shape[0])

```

```

239
240
241     ##Get columns
242     columns_n = []
243     #set the amount of lines by defining stepsize in range(0,xsize, xsize/XXX)
244     for i in range(0,xsize_n):
245         columns_n.append(impixels_n[:,i])
246     columns_n=np.array(columns_n)
247
248     #columns.shape yields (x,y) means I have x columns of a length of y
249     amount_columns_n = int(columns_n.shape[0]) #lines earlier
250     length_columns_n = int(columns_n.shape[1]) #length earlier
251
252
253     ##Average columns
254     #summing pixels of every column
255     sum_n = [] # gives single column with sum of all lines
256     for j in range(0,length_columns_n):
257         x = columns_n[0,j]
258         for i in range(1,amount_columns_n-1):
259             x = x + columns_n[i,j]
260         sum_n.append(x)
261
262     sum_n = np.array(sum_n)
263
264     #dividing by amount of columns
265     avercolumn_n = sum_n/amount_columns_n
266
267     ##background subtraction
268     avercolumn_n = (avercolumn_n - bg)/bg
269
270     #set negative pixels to zero
271     for i in range(0,length_columns_n):
272         if avercolumn_n[i]<0:
273             avercolumn_n[i]=0
274
275     ##Averaging total intensity
276     #calculating total intensity value divided by length of column (=width of area)
277     tot_inten_value_n = float(np.sum(avercolumn_n))/float(len(avercolumn_n))
278
279     """Illustration of spatial intensity distribution in y"""
280     if plot_y_inten==True:
281
282         if same_graph_y == True:
283             plt.figure(fig_y_inten_distr)
284             x = np.arange(0,length_columns)
285             y = avercolumn
286             plt.plot(x,y,label=imname[6:9]+" bg= "+str(int(bg)))
287             plt.xlabel("ypixel from top to bottom of image")
288             plt.ylabel("average intensity")
289             plt.title("average intensity over y-axis for "+imname[0:5]+imname[9:22])
290             plt.legend()
291             plt.savefig("y_intensity_distribution"+imname[0:4]+imname[9:22])
292             if imname == name_sets[index_acquisitionset][-1]:
293                 plt.close(fig_y_inten_distr)
294             else:
295                 pass
296
297         else:
298             fig = plt.figure()
299             x = np.arange(0,length_columns)
300             y = avercolumn
301             plt.plot(x,y,label=imname[6:8])
302             plt.xlabel("ypixel from top to bottom of image")
303             plt.ylabel("average intensity")
304             plt.title("average intensity over y-axis of "+imname)
305             plt.figtext(.7, .8, "bg= "+str(int(bg)))
306             plt.savefig(str(imname)+"_y_intensity_distribution")
307             plt.close (fig)
308

```

```

309     else:
310         pass
311
312     """Averaging total intensity of picture"""
313     #cropping averaged column to y-pixels that contain worm: [x0-3sigma, x0+3sigma]
314     x = avercolumn[int(popt[1]-3*popt[2]):int(popt[1]+popt[2])]
315     #total intensity divided by length of column (=width of worm)
316     tot_inten_value = float(np.sum(x))/float(len(x))
317
318     """Signal-to-noise-ratio"""
319     snratio = float(tot_inten_value_n)/float(tot_inten_value)
320     totintensity_sn.append(snratio)
321     calc_stats_sn.append(snratio)
322
323     """statistics on each acquisition set"""
324     name_sets=np.array(name_sets,dtype=object)
325     totintensity_sn = [] #list of total intensity values for each image
326     stats_acquisitions_sn = [] #list of statistical values for each acquisition set
327     calc_stats_sn = [] #list for calculating statistical values of each acquisition set
328
329
330 for index_acquisitionset in range(0,len(name_sets),2): #loop through acquisition sets
331     print("Set of " + str(name_sets[index_acquisitionset][1][0:6])+str(name_sets[
332         index_acquisitionset][1][10:22]))
333     for j in range(0,len(name_sets[index_acquisitionset])): #loop through images of one set
334         imname= name_sets[index_acquisitionset][j]
335         imname_n = name_sets[index_acquisitionset + 1][j]
336         print("image", imname)
337
338         process(imname,imname_n,index_acquisitionset) #add snratio to totintensity-list for
339         #if last image of set reached, determine statistics: stats_acquisitions=[median_set1,median_dev_set1, med_set2,med_dev_set2,...]
340         if imname == name_sets[index_acquisitionset][-1]:
341             median = np.median(calc_stats_sn)
342             print("Median=",median)
343             stats_acquisitions_sn.append(median)
344             mean = np.mean(calc_stats_sn)
345             print("Mean=",mean)
346             std = np.std(calc_stats_sn)
347             print("std=",std)
348             meddev = robust.mad(calc_stats_sn)
349             stats_acquisitions_sn.append(meddev)
350
351             calc_stats_sn = [] #after acquisition set fully processed, clear data
352         else:
353             pass
354
355
356     """plotting statistics"""
357     if plot_stats== True:
358         #median values
359         means_sn=np.array(stats_acquisitions_sn[0:len(stats_acquisitions_sn):2])
360         #median deviations as errors
361         std_sn=np.array(stats_acquisitions_sn[1:len(stats_acquisitions_sn):2])
362         #time points
363         t = []
364         for i in range(0,len(time_sets)):
365             t.append(time_sets[i][0]) #append first time point for each acquisition set
366         t=np.array(t)
367
368         ##plot figure
369         plt.figure(fig_snratio_stats)
370         plt.errorbar(t, means_sn, std_sn, linestyle='None', marker='x')
371         plt.xlabel("time[hrs]")
372         plt.ylabel("total intensity")
373         plt.title("signal-to-noise ratio over time")
374         plt.savefig("snratio_over_time_stats_"+imname[0:6]+imname[10:22])
375         plt.close(fig_snratio_stats)

```

```

376     else:
377         pass
378
379     """Plotting total intensity over time"""
380     if plot_points==True:
381         plt.figure(fig_snratio_points)
382         totintensity = np.array(totintensity_sn)
383         plt.errorbar(time,totintensity_sn,linestyle='None', marker='x')
384         plt.xlabel("time[hrs]")
385         plt.ylabel("signal-to-noise ratio")
386         plt.title("signal-to-noise ratio of over time")
387         plt.savefig("sn_ratio_time_points_"+imname[0:6]+imname[10:22])
388         plt.close(fig_snratio_points)
389     else:
390         pass
391
392 if plot_both == True:
393
394     plt.figure(fig_snratio)
395
396     ##prepare data
397     #median values
398     means_sn=np.array(stats_acquisitions_sn[0:len(stats_acquisitions_sn):2])
399     #median deviations as errors
400     std_sn=np.array(stats_acquisitions_sn[1:len(stats_acquisitions_sn):2])
401     #time points
402     t = []
403     for i in range(0,len(time_sets)):
404         t.append(time_sets[i][0]) #append first time point for each acquisition set
405     t=np.array(t)
406
407     totintensity_sn = np.array(totintensity_sn)
408
409     ##plot both graphs
410     plt.subplot(2,1,1)
411     plt.scatter(time,totintensity_sn, linestyle='None', marker='x')
412     plt.ylabel("signal-to-noise ratio")
413     plt.title("signal-to-noise ratio of over time")
414
415     plt.subplot(2, 1, 2)
416     plt.errorbar(t, means_sn, std_sn, linestyle='None', marker='x')
417     plt.xlabel("time[hrs]")
418     plt.ylabel("signal-to-noise ratio")
419
420     plt.savefig("snratio_over_time_"+imname[0:6]+imname[10:22])
421     plt.close(fig_snratio)

```

Title page figures

left: Heidelberg University[66]

right: Institute of Photonic Sciences: Neurophotonics and Mechanical Systems Biology[67]

References

- [1] History of microscopy – timeline. <https://www.sciencelearn.org.nz/resources/1692-history-of-microscopy-timeline>, 23.02.21 2:44 PM.
- [2] Malte Renz. Fluorescence microscopy—a historical and technical perspective. *WormBook*, ed. *The C. elegans Research Community*, 12 April 2013.
- [3] Roohullah Hemmati Rodney B. Luword Khosro Khajehe Sana Sharifiana, Ahmad Homaeib. The emerging use of bioluminescence in medical research. *Biomedicine Pharmacotherapy*, 101:74–68, May 2018.
- [4] Wightman B. Corsi A.K. and Chalfie M. A transparent window into biology: A primer on caenorhabditis elegans. *The C. elegans Research Community, WormBook*, June 18, 2015.
- [5] Heidi Tissenbaum Kelvin Yen, Sri Devi Narasimhan. Daf-16/forkhead box o transcription factor: Many paths to a single fork(head) in the road. *Chemical Physics*, 14:623–34, February 2011.
- [6] S. Brenner. The genetics of caenorhabditis elegans. *Genetics*, 77:71—94, May 1974.
- [7] Thomson JN Brenner S White JG, Southgate E. The structure of the nervous system of the nematode caenorhabditis elegans. *Philosophical Transactions of the Royal Society of London.*, 1165:1—340, November 1986.
- [8] Wightman B. Corsi A.K. and Chalfie M. A. A transparent window into biology: A primer on caenorhabditis elegans. *WormBook*, ed. *The C. elegans Research Community*, June 18, 2015.
- [9] Amita Pandey. The unc-53 mediated interactome. *SpringerBriefs in Neuroscience*, July 2014.
- [10] M.B. Goodman. Mechanosensation. *WormBook*, ed. *The C. elegans Research Community*, January 06, 2006.
- [11] M. Chalfie and J. Sulston. Developmental genetics of the mechanosensory neurons of caenorhabditis elegans. *Dev. Biol.*, 82:358–370, 1981.
- [12] G. G. Stokes. *On the Change of Refrangibility of Light*. Philosophical Transactions of the Royal Society of London, 1852.
- [13] Chan Im Chunyan Chi and Gerhard Wegnera. Lifetime determination of fluorescence and phosphorescence of a series of oligofluorenes. *J. Chem. Phys.*, 124, 2006.
- [14] J. Hofkens M. Sauer and J. Enderlein. *Handbook of Fluorescence Spectroscopy and Imaging*. WILEY-VCH Verlag GmbH Co. KGaA, Weinheim, 2011.
- [15] Lei Xu. *Development and application of ultra-sensitive fluorescence spectroscopy and microscopy for biomolecular interaction studies*. PhD thesis, KTH Applied Physics AlbaNova University Center Experimental Biomolecular Physics, 2014.
- [16] V. Ramamurthy N.J. Turro and J.C. Scaiano. Principles of molecular photochemistry: An introduction. *University Science Books*, 2009.
- [17] Michael Kasha. Characterization of electronic transitions in complex molecules. *Discussions of the Faraday Society*, 9:14–19, 1950.
- [18] J. R. Lakowicz. Introduction to fluorescence, principles of fluorescence spectroscopy. *Springer US*, 2006.

- [19] D. Davenport; J. A. C. Nicol. *Luminescence in Hydromedusae*. Philosophical Transactions of the Royal Society of London, 1955.
- [20] Y. Saiga O. Shimomura, F. H. Johnson. Extraction, purification and properties of aequorin, a bioluminescent protein from the luminous hydromedusan, aequorea. *J Cell Comp Physiol.*, 1962.
- [21] Christoph Eckert. Working with green fluorescent proteins: Tools and properties. Feb 7, 2019. <https://resources.chromotek.com/blog/green-fluorescent-proteins-tools>, last checked 11.02.2021 4:41PM.
- [22] G. N. Phillips Jr. F. Yang, L. G. Moss. The molecular structure of green fluorescent protein. *Nat Biotechnol.*, 1996 Oct.
- [23] Dr. Christoph Greb. Basic principles of luminescence. <https://www.leica-microsystems.com/science-lab/basic-principles-of-luminescence/>, last checked 08.02.2021.
- [24] A. Zumbusch G. Jung, C. Braeuchle. Two-color fluorescence correlation spectroscopy of one chromophore: Application to the e222q mutant of the green fluorescent protein. *The Journal of Chemical Physics*, 114(7):3149–3156, February 2001.
- [25] Koehler A. Gedanken zu einem neuen beleuchtungsverfahren für mikrophotographische zwecke. *Zeitschrift für wissenschaftliche Mikroskopie*, 1893.
- [26] Ian Parker Martin D. Bootman Michael J. Sanderson, Ian Smith. Fluorescence microscopy. *Cold Spring Harb Protoc.*, October 2014.
- [27] Max; Emil Wolf Born. *Principles of Optics*. 1997.
- [28] John E. Greivenkamp. *Field Guide to Geometrical Optics*. 20 January 2004.
- [29] C.J.R.Sheppard. Microscopy — overview. *Encyclopedia of Modern Optics*, pages 61–69, 2005.
- [30] Michelle Arkin Douglas Auld Chris Austin Bruce Bejcek Marcie Glicksman James Inglese Vance Lemmon Zhuyin Li James McGee Owen McManus Lisa Minor Andrew Napper Terry Riss O. Joseph Trask Jeff Weidner G. Sitta Sittampalam, Neely Gal-Edd. *Assay Guidance Manual*. Eli Lilly Company and the National Center for Advancing Translational Sciences.
- [31] Harekrushna Sahoo. Fluorescent labeling techniques in biomolecules: a flashback. *RSC Advances*, 18:7017—7029, 1 January 2012.
- [32] Nathalie; Christiane Delarbre; Gabriel Gachelin; Vincent Laudet Spruyt. Complete sequence of the amphioxus (branchiostoma lanceolatum) mitochondrial genome: relations to vertebrates. *Nucleic Acids Research*, 26:3279—3285, 1998.
- [33] Charles Harmin. *Systematics of the order Corallimorpharia*. University of Kansas, 2007.
- [34] Gotthard G. von Stetten D. De Sanctis D. Pasquier H. Lambert G.G. Shaner N.C. Royant A. Clavel, D. Structural analysis of the bright monomeric yellow-green fluorescent protein mneongreen obtained by directed evolution. *Acta Crystallogr D Struct Biol*, 72:1298–1307, 2016.
- [35] Peter Schultz Petra Schwille Thomas Weidemann Frederik Steiert, Eugene P. Petrov. Photophysical behavior of mneongreen, an evolutionarily distant green fluorescent protein. *Biophysical Journal*, 114:2419–2431, 22 May 2018.
- [36] Branchiostoma lanceolatum. <http://marimba.obs-vlfr.fr/organism/Branchiostoma/lanceolatum>, last checked 13.02.21 7:23 PM.
- [37] Miriam B Goodman Robert O'Hagan, Martin Chalfie. The mec-4 deg/enac channel of caenorhabditis elegans touch receptor neurons transduces mechanical signals. *Nat Neurosci.*, 8:43–50, 2005.
- [38] V Plunger A Aryana A Fire P G Okkema, S W Harrison. Sequence requirements for myosin gene expression and regulation in caenorhabditis elegans. *Genetics*, 135:385–404, 1993 Oct.

- [39] Paul Davis. Nomenclature — genotypes. *WormBase*, 2018. <https://wormbase.org/about/userguide/nomenclature#c59731f4jd1e0imabg86k2h--10>.
- [40] Reto Gassmann Iain Cheeseman Paul Maddox Shirin Bahmanyar Ana Carvalho Sherry Niessen John R. Yates Karen Oegema Arshad Desai Esther Zanin, Julien Dumont.
- [41] Asako Sugimoto Mika Toya, Yumi Iida. Imaging of mitotic spindle dynamics in *caenorhabditis elegans* embryos. *Methods in Cell Biology*, 97:259–372, 2010.
- [42] Peter Meister Peter Askjaer, Vincent Galy. Modern tools to study nuclear pore complexes and nucleocytoplasmic transport in *caenorhabditis elegans*. *Methods in Cell Biology*, 122:277–310, 2014.
- [43] T. C. MEvans.
- [44] C. Mello and A. Fire. Dna transformation. *Methods Cell Biol.*, 48:452–482, 1995.
- [45] Harald Hutter. *Caenorhabditis elegans: Cell biology and physiology*. *Methods in Cell Biology*, 107:67–92, 2012.
- [46] Kazuki Horikawa Noriyuki Hatsugai Yuriko Higuchi Mitsuru Hashida Yu Yoshida Tomoki Matsuda Yoshiyuki Arai Takeharu Nagai Kenta Saito, Y.-F. Chang. Luminescent proteins for high-speed single-cell and whole-body imaging. *Nature Communications*, 2012.
- [47] Pavel Tomancak Emmanuel G Reynaud Hari Shroff P Philippe Laissie, Rana A Alghamdi. Assessing phototoxicity in live fluorescence imaging. *Nature Methods*, 2017.
- [48] Travis Mazer Zachary Pincus and Frank J. Slack. Autofluorescence as a measure of senescence in *c. elegans*: look to red, not blue or green. *Aging (Albany NY)*, 2016.
- [49] John Lee. Bioluminescence, the nature of the light. *The University of Georgia*, 2017.
- [50] Osamu Shimomura. *Bioluminescence: Chemical Principles and Methods*. 2006.
- [51] Southworth T. L. Murtiashaw M. H. Boije H. Fleet Branchini, B. R. A mutagenesis study of the putative luciferin binding site residues of firefly luciferase. *Biochemistry*, 42:10429—10436, 2003.
- [52] Baubet. Chimeric green fluorescent protein-aequorin as bioluminescent ca²⁺ reporters at the single-cell level. *Proc. Natl Acad. Sci. USA*, 97:7260—7265, 2000.
- [53] Fenn T. D. Wu A. M. Gambhir Loening, A. M. Consensus guided mutagenesis of renilla luciferase yields enhanced stability and light output. *Prot. Eng. Des. Sel.*, 19:391—400, 2006.
- [54] Colin A Flaveny Weimin Li Adele M Musicant Sany Hoxha Min Guo John L Cleveland Franz X Schaub, Md Shamim Reza and Antonio L Amelio6. Fluorophore-nanoluc bret reporters enable sensitive in vivo optical imaging and flow cytometry for monitoring tumorigenesis. *Cancer Res.*, 75:5023—5033, 2015 Dec.
- [55] W. W. Cormier Ward. In vitro energy transfer in renilla bioluminescence. *J. Phys. Chem.*, 80:2289—2291, 1967.
- [56] David S. Bradshaw David L. Andrews. Virtual photons, dipole fields and energy transfer: a quantum electrodynamical approach. *European Journal of Physics*, 25:845—858, 2004.
- [57] D.L. Andrews. A unified theory of radiative and radiationless molecular energy transfer. *Chemical Physics*, 135:195–201, March 1989.
- [58] D. Klostermeier S. Hartmann. Single-molecule enzymology: Fluorescence-based and high-throughput methods. *Methods in Enzymology*, 2016.
- [59] Theresa Stiernagle. Maintenance of *c. elegans*. *WormBook*, February 11, 2006.
- [60] Cassandra Coburn and David Gems. The mysterious case of the *c. elegans* gut granule: death fluorescence, anthranilic acid and the kynurenine pathway. *Front. Genet.*, 07 August 2013.

- [61] Coburn C. Anthranilate fluorescence marks a calciumpropagated necrotic wave that promotes organismal death in *c. elegans*. *PLoS Biol*, 2013.
- [62] Monica Monici. Cell and tissue autofluorescence research and diagnostic applications. *Biotechnology Annual Review*, pages 227–256, 2005.
- [63] Yin DZ and Brunk UT. Microfluorometric and fluorometric lipofuscin spectral discrepancies: a concentration-dependent metachromatic effect? *Mech Ageing Dev.*, 59:95—109, 1991.
- [64] Bader N. Jung, T. and T. Grune. Lipofuscin: formation, distribution, and metabolic consequences. *Ann. N. Y. Acad. Sci.*, 1119:97—111, 2007.
- [65] Guy A. Caldwell Kim A. Caldwell, Corey W. Willicott. Modeling neurodegeneration in *caenorhabditis elegans*. *Disease Models Mechanisms*, 26 October 2020.
- [66] Heidelberg university. <https://www.uni-heidelberg.de/en>, last checked 24.02.21 11:20 AM.
- [67] Neurophotonics and mechanical systems biology - icfo. <http://livinglight.icfo.eu/>, last checked 24.02.21 11:18 AM.